

# Paleoceanography and Paleoclimatology®



## RESEARCH ARTICLE

10.1029/2024PA005041

### Key Points:

- *Chaetoceros* resting spores record  $\delta^{15}\text{N}_{\text{DB}}$  values lower than other diatoms in marine sediment and in laboratory culture
- The N isotopic offset of *Chaetoceros* resting spores relative to other diatoms ranges from 1.1–8.2‰
- Changes in relative abundance over time will not bias paleo records if the change in relative surface area contribution is below ~5%

### Supporting Information:

Supporting Information may be found in the online version of this article.

### Correspondence to:

I. A. Dove,  
isabel\_dove@uri.edu

### Citation:

Dove, I. A., Bishop, I. W., Crosta, X., Riedinger, N., Kelly, R. P., & Robinson, R. S. (2025). *Chaetoceros* resting spores do not significantly bias sedimentary diatom-bound nitrogen isotope records despite distinctly low values.

*Paleoceanography and Paleoclimatology*, 40, e2024PA005041. <https://doi.org/10.1029/2024PA005041>

Received 15 OCT 2024

Accepted 21 MAR 2025

## *Chaetoceros* Resting Spores Do Not Significantly Bias Sedimentary Diatom-Bound Nitrogen Isotope Records Despite Distinctly Low Values

I. A. Dove<sup>1</sup> , I. W. Bishop<sup>1,2</sup>, X. Crosta<sup>3</sup>, N. Riedinger<sup>4</sup> , R. P. Kelly<sup>1</sup> , and R. S. Robinson<sup>1</sup> 

<sup>1</sup>Graduate School of Oceanography, University of Rhode Island, Narragansett, RI, USA, <sup>2</sup>Now at U.S. Geological Survey, Southwest Biological Science Center, Grand Canyon Monitoring and Research Center, Flagstaff, AZ, USA, <sup>3</sup>Université de Bordeaux, CNRS, EPHE, UMR 5805 EPOC, Pessac, France, <sup>4</sup>Boone Pickens School of Geology, Oklahoma State University, Stillwater, OK, USA

**Abstract** The nitrogen isotopic composition of diatom frustule-bound organic matter ( $\delta^{15}\text{N}_{\text{DB}}$ ) is often used to study changes in high latitude biological pump efficiency across glacial-interglacial cycles, but the proxy may be biased by species-specific effects. The genus *Chaetoceros* is of particular interest because of its abundance throughout ocean basins, its shifting biogeography during glacial periods, and the ability of many species to form heavily silicified resting spores. Here we investigate how *Chaetoceros* resting spores (CRS) record surface nitrate conditions in their nitrogen isotopic composition, and thus impact  $\delta^{15}\text{N}_{\text{DB}}$  records, using assemblage-specific sedimentary  $\delta^{15}\text{N}_{\text{DB}}$  measurements and laboratory culture experiments. We find that fossil CRS from ODP Site 1098 record  $\delta^{15}\text{N}_{\text{DB}}$  values 1.1–7.8‰ lower than non-CRS diatoms in sediment. CRS grown in culture yield consistent results, recording  $\delta^{15}\text{N}_{\text{DB}}$  values 2.6–8.2‰ lower than vegetative *Chaetoceros* in the same cultures. Low values are attributed to assimilation of isotopically light ammonium, heavy silicification, and/or internal nitrogen allocation processes during sporulation. Applying these findings to published  $\delta^{15}\text{N}_{\text{DB}}$  records, variable CRS relative abundance in open ocean glacial sediments does not significantly bias  $\delta^{15}\text{N}_{\text{DB}}$  records across glacial-interglacial cycles, despite the large  $\delta^{15}\text{N}_{\text{DB}}$  difference observed in CRS versus non-CRS diatoms, due to the spores' small size.

## 1. Introduction

Modulations in high-latitude biological pump efficiency have long been recognized as a potential driver of glacial-interglacial cycles (Knox & McElroy, 1984; Sarmiento & Toggweiler, 1984; Siegenthaler & Wenk, 1984), with fossil-bound nitrogen (N) isotope records suggesting that a more efficient biological pump played a role in lowering glacial atmospheric  $\text{CO}_2$  (Ai et al., 2020; Martínez-García et al., 2014; Robinson et al., 2005; Robinson & Sigman, 2008; Sigman et al., 1999; Studer et al., 2015). However, these records are limited by uncertainties around species-related influences (e.g., Horn, Beucher, et al., 2011) and geographic coverage, as there are no published records from highly productive regions proximal to the Antarctic coast. Published records are presently limited to closer to the core of the upwelling region within the Antarctic Zone of the Southern Ocean (Figure 1), where wind-driven upwelling brings nutrient- and  $\text{CO}_2$ -rich waters to the surface. Nutrients are partially consumed by phytoplankton, due to iron and light limitation (Martin, 1990; Mitchell et al., 1991), and advected laterally. This incomplete nutrient utilization results in inefficient export and sequestered  $\text{CO}_2$  leaking back into the atmosphere (Sigman et al., 2010).

Changes in relative nutrient utilization in the nitrate-replete Antarctic Zone, and therefore changes in biological pump efficiency, can be investigated via sedimentary N isotope records. The isotopic composition of N ( $\delta^{15}\text{N}$ ) in sediments reflects the preferential uptake of nitrate containing  $^{14}\text{N}$  by phytoplankton, leaving behind a nutrient pool enriched in  $^{15}\text{N}$ -containing nitrate (Wada & Hattori, 1978). As nitrate consumption progresses, the N isotopic composition of both the nitrate pool and the resulting organic matter becomes progressively enriched in  $^{15}\text{N}$ , with the higher  $\delta^{15}\text{N}$  value of sinking organic matter reflecting enhanced nitrate utilization (Altabet & Francois, 1994). Fossil-bound N isotope records are preferred for paleoceanographic analyses as the organic N bound with biominerals is purportedly protected from alteration (Robinson et al., 2004, 2020; Sigman et al., 1999). Diatoms, which are single-celled algae characterized by their opaline frustules, are the ideal microfossil group with which to generate fossil-bound  $\delta^{15}\text{N}$  records in the Southern Ocean due to their abundance in surface water and in sediments. Diatoms are the dominant type of phytoplankton in the Antarctic Zone of the Southern Ocean

© 2025. The Author(s).

This is an open access article under the terms of the [Creative Commons Attribution-NonCommercial-NoDerivs License](#), which permits use and distribution in any medium, provided the original work is properly cited, the use is non-commercial and no modifications or adaptations are made.

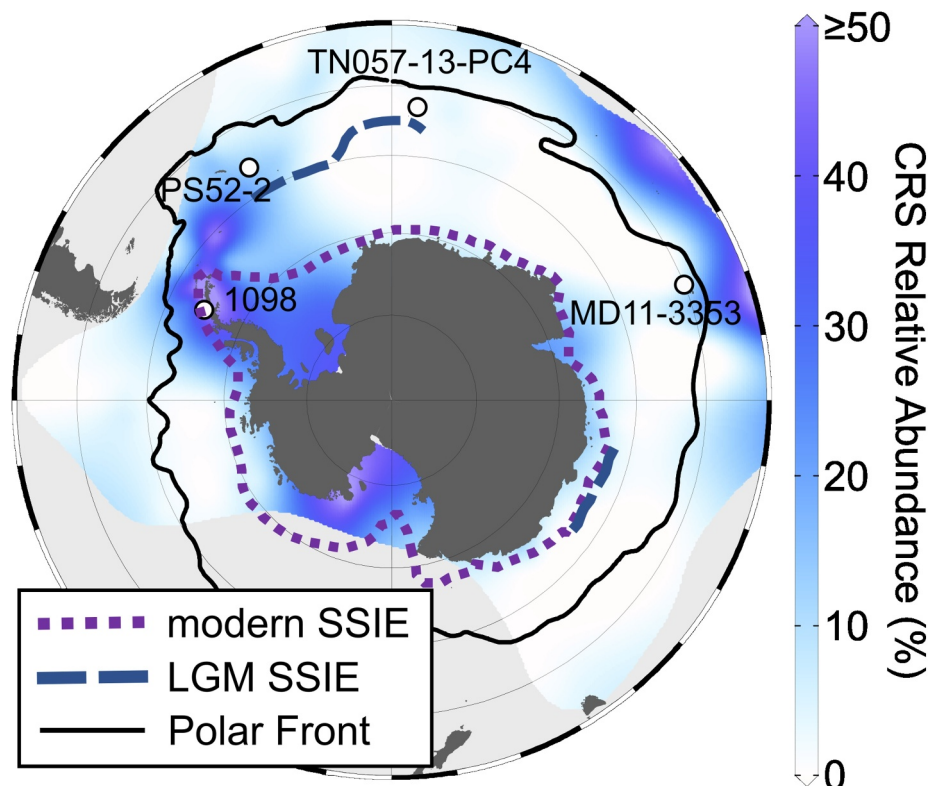


**Figure 1.** Relative abundance (%) of CRS in modern Southern Ocean sediments (Armand et al., 2005; Crosta et al., 1997; Esper et al., 2010) and location of sediment cores PS119 Site 52-2, ODP Site 1098, TN057-13-PC4, and MD11-3353. Gray shading indicates regions with no CRS data. Dashed blue lines indicate the summer sea ice edge (SSIE) during the last glacial maximum (Gersonde et al., 2005), dotted purple line indicates the modern summer sea ice edge (Schweitzer, 1995), and solid black line represents the northern boundary of the modern Antarctic Zone (Orsi et al., 1995).

and are primary contributors to the Southern Ocean biological pump (Rigual-Hernández et al., 2015; Smetacek et al., 2012). The efficiency with which diatoms export carbon depends on many factors including size and morphology (Tréguer et al., 2018), along with the aforementioned effect of nutrient supply. While diatom frustules are primarily composed of biogenic silica, they contain structural proteins and polyamines that comprise the N pool from which diatom-bound N isotopes ( $\delta^{15}\text{N}_{\text{DB}}$ ) are measured (Hildebrand et al., 2018; Kröger et al., 1999, 2000; Sumper & Kröger, 2004).

Despite its proven utility, the  $\delta^{15}\text{N}_{\text{DB}}$  proxy may suffer from species-specific biases. Sedimentary  $\delta^{15}\text{N}_{\text{DB}}$  records integrate nutrient-nitrogen fractionation signals from all diatom species present in a given sample and therefore may be affected by community composition (Horn, Beucher, et al., 2011; Jacot Des Combes et al., 2008; Studer et al., 2013, 2015). Different diatom species contain varying proportions of N-bearing organic compounds with distinct fractionations and thus isotopic compositions within their frustules, resulting in a possible species-specific relationship between  $\delta^{15}\text{N}_{\text{biomass}}$  and  $\delta^{15}\text{N}_{\text{DB}}$  (Horn, Robinson, et al., 2011; Jones et al., 2022). The offset between  $\delta^{15}\text{N}_{\text{biomass}}$  and  $\delta^{15}\text{N}_{\text{DB}}$  of a given species, or  $\epsilon_{\text{DB}}$ , signifies differences in how biochemical reactions fractionate N into diatom frustules' organic matrices. Recent field and culture work suggest negative values of  $\epsilon_{\text{DB}}$  ( $\delta^{15}\text{N}_{\text{biomass}} < \delta^{15}\text{N}_{\text{DB}}$ ), while sediment-based work suggests potential species-specific offsets (Jones et al., 2022; Robinson et al., 2020; Studer et al., 2015). Improving geographic coverage of  $\delta^{15}\text{N}_{\text{DB}}$  records requires that we further examine how the  $\delta^{15}\text{N}_{\text{DB}}$  of certain diatom species relates to the surface nutrient conditions of the ocean in which they grew.

The diatom genus *Chaetoceros* is particularly relevant because it is a prominent component of Southern Ocean diatom assemblages, particularly in coastal areas, and plays an important role in exporting carbon to the deep ocean (Rembauville et al., 2016). Many species of the *Chaetoceros* subgenus *Hyalochaete* form robust resting spores (herein CRS) as a survival strategy in response to adverse conditions such as nutrient or light limitation

(French & Hargraves, 1985; Oku & Kamatani, 1997; Pelusi et al., 2020). In contrast to weakly silicified vegetative cells of *Chaetoceros* subg. *Hyalochaete*, CRS are heavily silicified. Laboratory-based experiments show that frustule dissolution may bias Southern Ocean sedimentary diatom assemblages, with vegetative *Chaetoceros* frustules being more readily dissolved than resting spores (Crosta et al., 1997; Pichon et al., 1992). Additionally, sediment trap records from both the North Atlantic and the Southern Ocean show that the relative proportion of resting spores within sinking diatom assemblages increases with depth due to enhanced preservation of robust frustules (Rembauville et al., 2016; Rynearson et al., 2013). Because CRS likely form under nutrient-depleted conditions (in which nitrate is enriched in  $^{15}\text{N}$ ) and because they are preferentially preserved in marine sediments, we hypothesize that they might bias records toward higher  $\delta^{15}\text{N}_{\text{DB}}$  values, which signal a greater degree of nutrient utilization.

CRS microfossils are common in Southern Ocean marine sediments and are associated with coastal settings both around Antarctica and subantarctic islands, but their relative abundance varies across time and space (Armand et al., 2005; Crosta et al., 1997; Esper et al., 2010; Zielinski & Gersonde, 1997; Figure 1). Around Antarctica, they are associated with sea ice, as modern sediment trap data show blooms co-occurring with melting sea ice in the austral spring (Leventer, 1991). Furthermore, laminated coastal sediments suggest seasonal CRS deposition following sea ice retreat (Denis et al., 2006; Maddison et al., 2005). Importantly, the relative abundance of CRS increases in pelagic sediments during glacial intervals due to northward expansion of the sea ice edge (Abelmann et al., 2006). Therefore, increased CRS relative abundance in glacial sediments could bias Antarctic Zone  $\delta^{15}\text{N}_{\text{DB}}$  records spanning glacial-interglacial cycles.

Here we present  $\delta^{15}\text{N}_{\text{DB}}$  values measured from isolated sedimentary CRS and laboratory culture experiments to characterize how CRS record surface nutrient conditions in their N isotopic composition. For the culture work, wild type *C. socialis* were resurrected from resting spores in Southern Ocean surface sediment and induced back into resting spores by nitrate limitation. We apply our findings to reevaluate relevant published  $\delta^{15}\text{N}_{\text{DB}}$  records that have accompanying diatom assemblage data, spanning glacial-interglacial cycles. Contrary to expectations, we find that CRS record low  $\delta^{15}\text{N}_{\text{DB}}$  values relative to vegetative cells and non-*Chaetoceros* diatoms, potentially biasing  $\delta^{15}\text{N}_{\text{DB}}$  measurements toward lower values and therefore leading to underestimates of the role of the biological pump in lowering glacial atmospheric  $\text{CO}_2$ . Mass balance calculations using published diatom community assemblages over glacial-interglacial cycles suggest that only large changes in CRS relative abundance, equating to roughly 5% changes in relative surface area contribution, significantly bias  $\delta^{15}\text{N}_{\text{DB}}$  records.

## 2. Material and Methods

### 2.1. Sedimentary CRS Analysis

Sedimentary CRS provide a field-based view of how CRS record surface ocean nutrient conditions in their N isotopic composition. Laminated deglacial sediments at ODP Site 1098 (64.86°S, 64.21°W, 1,012 m depth; Figure 1) contain nearly monogeneric layers of CRS deposited during the austral spring (Maddison et al., 2005). Layers deposited during the summer contain a more diverse diatom assemblage but are still CRS-rich. We measured  $\delta^{15}\text{N}_{\text{DB}}$  from both the bulk diatom assemblage and isolated CRS within six spring laminae and six summer laminae to quantify assemblage-specific differences in  $\delta^{15}\text{N}_{\text{DB}}$ .

Samples were taken from a u-channel from core ODP1098B-5H-7. Laminae were visually identified and differentiated by season with color, as spring laminae are a lighter orange-brown and summer laminae are a darker blue-gray (Maddison et al., 2005), and confirmed with smear slides showing the diatom assemblage and terrigenous material in subsamples. A small spatula was used to separate laminae, and the edges of each lamina were scraped away in order to avoid cross-contamination of spring and summer samples.

#### 2.1.1. Sedimentary Diatom-Bound N Isotope Analysis

All sedimentary  $\delta^{15}\text{N}_{\text{DB}}$  samples were sieved at 63  $\mu\text{m}$ , using the <63  $\mu\text{m}$  fraction for the bulk diatom assemblage  $\delta^{15}\text{N}_{\text{DB}}$  measurements. Subsamples for CRS-specific  $\delta^{15}\text{N}_{\text{DB}}$  measurements were further processed following the methods of Egan et al. (2012) and Swann et al. (2013), in which subsamples of the <63  $\mu\text{m}$  fraction were filtered through a 10  $\mu\text{m}$  Nitex mesh in a gentle ultrasonic bath. The resulting <10  $\mu\text{m}$  fraction was dominated by CRS, but vegetative *Chaetoceros* were also present in similar proportions as in unseparated samples (Figure S1 in Supporting Information S1).

Both the bulk diatom assemblage and isolated CRS samples were prepared for  $\delta^{15}\text{N}_{\text{DB}}$  analysis following the method described in Horn, Beucher, et al. (2011). First, lithogenic material was removed by heavy liquid separation and adsorbed metals were removed with a reductive cleaning step using a sodium dithionite solution. Next, external organic matter was removed by permanganate oxidation, using sulfuric acid, saturated potassium permanganate, and saturated oxalic acid solutions. Finally, samples were treated with weak (14%) and strong (70%) perchloric acid solutions in a 100°C water bath to remove any remaining external organic matter.

Following chemical cleaning, dry samples were dissolved in a 0.22 M potassium persulfate and 1.5 M sodium hydroxide solution and organic frustule-bound N was oxidized to nitrate (Robinson et al., 2004).  $\delta^{15}\text{N}_{\text{DB}}$  values were then measured via the denitrifier method, in which nitrate is converted to nitrous oxide by denitrifying bacteria (Sigman et al., 2001). The  $\delta^{15}\text{N}_{\text{DB}}$  isotope ratio was measured by gas chromatography-isotope ratio mass spectrometry (GC-IRMS) on a Thermo Delta V IRMS and measurements were standardized with potassium nitrate reference materials IAEA-N3 and USGS34. Analytical precision, as determined by the pooled standard deviation of multiple measurements of replicate samples, is 0.4‰.

### 2.1.2. Diatom Community Composition and Surface Area Analysis

CRS contribution to diatom community composition was quantified in terms of relative abundance and relative surface area. Quantitative microscope slides of the <63  $\mu\text{m}$  fraction were made following the method of Scherer (1994). Diatom community composition was determined by identifying and counting at least 400 diatom valves at 1,000x magnification with immersion oil, following the technique of Crosta and Koç (2007). The CRS relative abundance was calculated by dividing CRS abundance by total diatom abundance.

To assess whether CRS bias sedimentary  $\delta^{15}\text{N}_{\text{DB}}$  records, it is essential to consider the relative amount of organic N that CRS contribute to the bulk diatom assemblage N pool. While CRS dominate the diatom assemblage in terms of relative numerical abundance, they are much smaller than other diatoms within the deglacial sediments from Site 1098, such as *Corethron* spp., *Coscinodiscus* spp., and *Thalassiosira antarctica* (Maddison et al., 2005; Taylor & Sjunneskog, 2002). Additionally, CRS vary greatly in size, with potentially orders of magnitude differences in cellular surface area and biovolume (Leblanc et al., 2012). Therefore, relative surface area is a more accurate measure of CRS contribution to the  $\delta^{15}\text{N}_{\text{DB}}$  signal than relative abundance. The two-dimensional surface area of all diatoms and of only CRS was measured following the method of Studer et al. (2013), in which 20 photomicrographs were taken at random for each sample at 400x magnification. Total diatom surface area and CRS-specific surface area was determined using ImageJ software by manually selecting all diatoms and then selecting only CRS. The CRS relative contribution for each sample was calculated by dividing CRS surface area by total diatom surface area.

## 2.2. Laboratory Cultures

### 2.2.1. Culture Material

Spore-forming *Chaetoceros* diatoms were grown in culture and induced into resting spores to characterize how CRS record nutrient utilization in their N isotopic composition in a controlled environment. Strains of spore forming *Chaetoceros* were obtained by isolating vegetative cells that germinated from sedimentary resting spores. Resting spore-rich surface sediments were retrieved by a multicore at site 52-2 of the *R/V Polarstern* expedition PS119 (Bohrmann, 2019) in the Scotia Sea (56.14°S, 31.48°W, 3,359 m water depth; Figure 1) and were stored in 50 mL centrifuge tubes in a dark refrigerator.

To induce germination, 1 mL of resting spore-rich sediment slurry was pipetted into 5 mL of sterile filtered *f/2* medium (Guillard, 1975). This inoculant was diluted by pipetting 500  $\mu\text{L}$  into another well with 5 mL of *f/2*. The resting spores were kept in a 4°C incubator at 24-hr continuous fluorescent light (50–70  $\mu\text{mol photons m}^{-2} \text{s}^{-1}$ ) and were periodically stirred gently and monitored for germination by light microscopy. Germination typically occurred within 4–8 weeks. Cells were then isolated in well plates and transferred to progressively larger volumes while in exponential growth phase. All experiments were conducted with strains of *C. socialis*, which were visually identified to the species level (Hasle & Syvertsen, 1997). Identification was confirmed by 18S rDNA sequence following the method of Bishop et al. (2022), the only difference being that rDNA was extracted using the Zymo Quick-DNA/RNA Miniprep Plus Kit, following the manufacturer's protocol. *Chaetoceros socialis* is an

ideal species with which to investigate the genus *Chaetoceros* because, within the genus, *C. socialis* is both the most abundant species and contributes the largest percentage to global diatom biomass (Leblanc et al., 2012).

### 2.2.2. Culture Experiments

Three experiments, each in triplicate, were conducted to characterize the N isotopic composition of vegetative *Chaetoceros* and CRS. Culture experiments were conducted in 20 L carboys to ensure sufficient material for  $\delta^{15}\text{N}_{\text{DB}}$  measurements. Carboys were filled with about 20 L of sterile filtered (0.2  $\mu\text{m}$ ) seawater from Narragansett Bay. Phosphate, silicic acid, trace metals, and vitamins were added at *f/2* concentrations, while nitrate was restricted to 45  $\mu\text{m}$  concentrations to induce resting spore formation. Previous studies have induced CRS formation with nitrate concentrations between 10 and 23  $\mu\text{m}$ , but we increased the concentration to obtain sufficient material for  $\delta^{15}\text{N}_{\text{DB}}$  measurements (Kuwata et al., 1993; Oku & Kamatani, 1997; Pelusi et al., 2020). Each carboy was inoculated with 200 mL of culture in exponential growth phase. Since the inoculant was grown in *f/2* medium, initial nutrient concentrations in the three carboys varied slightly and nitrate concentrations exceeded 45  $\mu\text{m}$ . Cultures were kept at 4°C with 24-hr continuous fluorescent light with 50–70  $\mu\text{mol photons m}^{-2} \text{ s}^{-1}$  intensity to simulate summertime Southern Ocean conditions and were continuously stirred and bubbled with filtered air. Cell growth was tracked via fluorescence and water samples were collected periodically throughout the experiment to track nutrient (silicic acid, ammonium, nitrate) utilization (Figure 2). Water samples were filtered and stored frozen until analysis, with subsamples acidified to pH 2 for ammonium concentration measurements. Approximately 5 mL of unfiltered water samples were also collected and preserved in a 2% acid Lugol's solution to monitor resting spore abundance. Cell counts were performed using a Sedgewick Rafter and a Nikon Eclipse E800 compound microscope under 200x magnification, with a minimum of 500 cells counted per sample.

We investigated the N isotopic composition of both vegetative *Chaetoceros* and CRS by harvesting cultures at two timepoints: before and after resting spore formation. Vegetative samples were collected by filtering biomass from approximately 10 L of each carboy prior to resting spore formation, 6–7 days after inoculation. Subsamples of 50 mL were filtered onto a precombusted GF/F filter for  $\delta^{15}\text{N}_{\text{biomass}}$  measurements. The remaining volume was filtered with 5  $\mu\text{m}$  polycarbonate filters for  $\delta^{15}\text{N}_{\text{DB}}$  measurements. All filters were kept frozen until analysis. Once a significant proportion of cells had sporulated, ~30 days later, CRS were harvested following the same procedure. The timing of sampling for each experiment is described in Supporting Information S1.

### 2.2.3. Dissolved Silica Measurements

Frozen water samples were gently thawed over a 24-hr period to avoid Si precipitation prior to dissolved silica (dSi) analysis. The dSi concentration was measured with a UV/Vis spectrophotometer following the colorimetric method of Strickland and Parsons (1972). Given high dSi concentrations in *f/2* medium, water samples collected early in the experiment were diluted to lower concentrations. Concentrations were calibrated with a sodium silicate dilution series ranging from 1.25 to 50  $\mu\text{m}$  and accuracy verified with the KANSO lot CH certified reference material. Analytical precision is 0.9  $\mu\text{m}$ .

### 2.2.4. Ammonium Concentration Measurements

Acidified water samples were analyzed for ammonium concentration following the fluorometric method of Holmes et al. (1999). 2 mL of each water sample was added to 8 mL of working reagent and incubated in the dark for 4 hr. Fluorescence was measured with the CDOM/ $\text{NH}_4$  optical package on a Turner Designs Trilogy Laboratory Fluorometer. Concentrations were calibrated with an ammonium chloride dilution series ranging from 0.25 to 5.0  $\mu\text{m}$ . Analytical precision is 0.4  $\mu\text{m}$ .

### 2.2.5. Nitrate Concentration and Isotope Analysis

Nitrate concentration in water samples was measured by chemiluminescent NO detection after conversion with a heated vanadium reagent using a Teledyne Instruments Model 200E chemiluminescence  $\text{NO}/\text{NO}_x$  analyzer (Braman & Hendrix, 1989). The N isotopic composition of nitrate ( $\delta^{15}\text{N}_{\text{NO}_3}$ ) was measured by the denitrifier method, as described above. Analytical precision is 0.2‰.

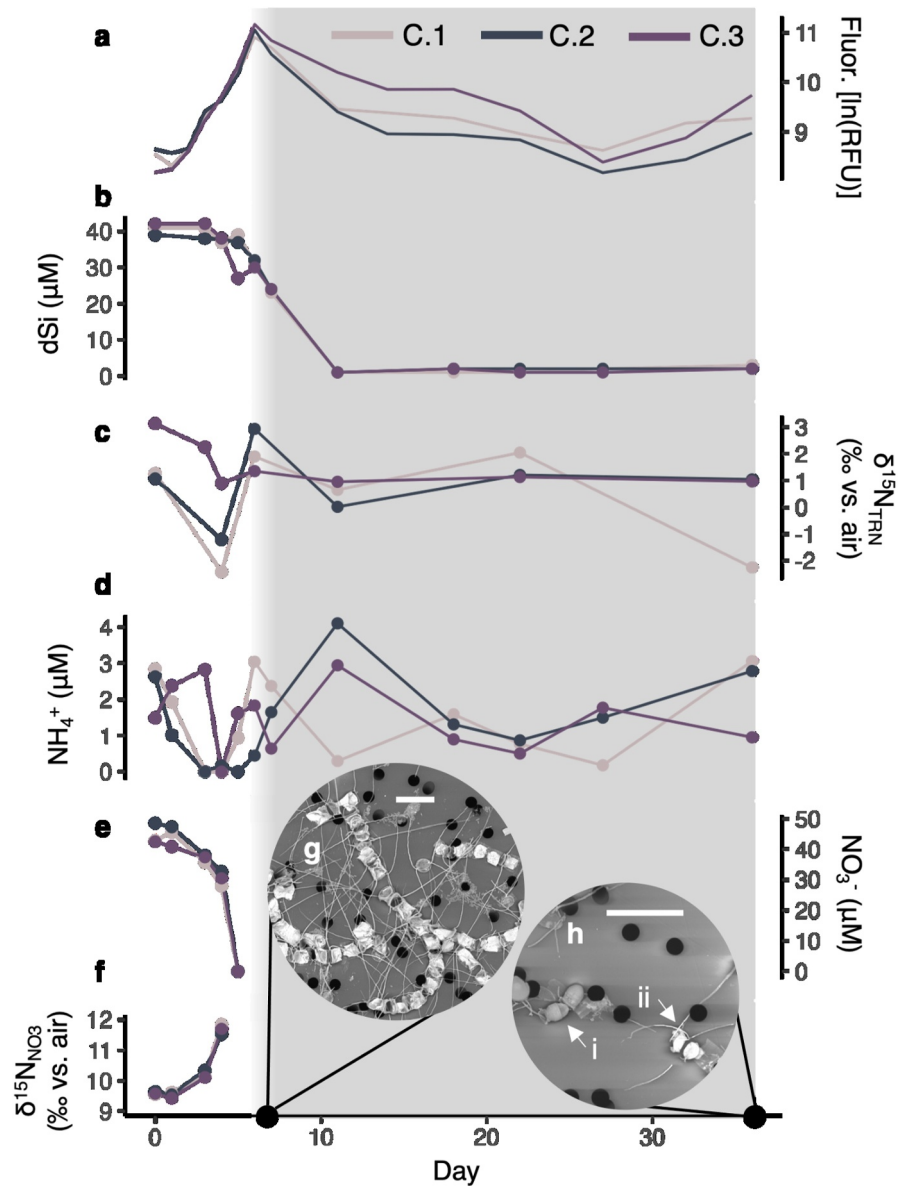


**Figure 2.** Culture growth and nutrient data tracked throughout experiment 3, color-coded by carboy (C.1-C.3). Growth is tracked via fluorescence and peaks when vegetative cells are harvested for isotopic analysis (a). Nutrients include dissolved Si (b), ammonium (d), and nitrate (e). The nitrogen isotopic composition of total reduced N (c) remains relatively constant while nitrate becomes progressively enriched in  $^{15}\text{N}$  (f). Gray shading indicates presence of CRS and the black circles denote the days when vegetative cells and resting spores are harvested. Insets are SEM images of culture subsamples collected on the days in which vegetative cells (g) and CRS (h) were harvested. Both CRS (h.i) and frustules from dead vegetative cells (h.ii) are present when CRS cultures are harvested. Scale bars are 20  $\mu\text{m}$ .

### 2.2.6. Total Reduced N Concentration and Isotope Analysis

Reduced N (ammonium and dissolved organic N) in water samples was oxidized to nitrate following a modified persulfate oxidation method (Knapp et al., 2005). A volume of 250  $\mu\text{L}$  of a 0.22 M potassium persulfate and 1.5 M sodium hydroxide solution was added to 1.5 mL of water sample and reacted in a pressure cooker (118°C) for one hour. Known amounts of the amino acid, glycine, were processed identically to ensure complete oxidation of reduced N. Following persulfate oxidation, nitrate concentration was measured by chemiluminescent NO detection. Total reduced N concentration was calculated by subtracting previously measured nitrate concentrations.

The N isotopic composition of oxidized samples was measured via the denitrifier method. A mass balance calculation using nitrate concentrations and  $\delta^{15}\text{N}_{\text{NO}_3}$  values from un-oxidized samples yielded the nitrogen isotopic composition of reduced N. Analytical precision is 0.3‰.

### 2.2.7. Biomass N Isotope Analysis

Dried GF/F filters were wrapped in tin capsules for  $\delta^{15}\text{N}_{\text{biomass}}$  analysis with a Costech 4,010 elemental analyzer coupled to a Thermo Delta V IRMS. Measurements were calibrated using reference materials IAEA N1 and N2 as well as an in-house aminocaproic acid standard. Analytical precision is 0.3‰.

### 2.2.8. Culture Diatom-Bound N Isotope Analysis

Vegetative and CRS samples were chemically cleaned for  $\delta^{15}\text{N}_{\text{DB}}$  analysis following the method of Morales et al. (2013). First, samples were repeatedly rinsed with a 2% sodium dodecyl sulfate (SDS) solution to remove weakly bound organic matter. Next, external organic matter was removed by the same cleaning steps as described above for sedimentary  $\delta^{15}\text{N}_{\text{DB}}$  samples.

Since frustules from dead vegetative cells remain in the carboys when the CRS sample is collected (Figure 2), additional treatment was required to isolate CRS. During the first two of the three culture experiments, we were unable to isolate CRS, instead collecting mixed vegetative and CRS samples. CRS were successfully isolated for  $\delta^{15}\text{N}_{\text{DB}}$  analysis during the third experiment. Following the SDS rinse, CRS samples were sonicated at 80 kHz to break the more fragile vegetative frustules. The sonicated samples were then filtered through a 5  $\mu\text{m}$  Nitex mesh. The >5  $\mu\text{m}$  fraction was left to settle in a 250 mL beaker filled with water for 2 hours. The samples were siphoned to ~40 mL, where only CRS remained (Figure S2 in Supporting Information S1).

Similar to the sedimentary samples, cleaned culture samples were dissolved and  $\delta^{15}\text{N}_{\text{DB}}$  values were measured by the persulfate-denitrifier method. The ratio of organic frustule-bound N to biogenic silica was calculated by dividing the volume-corrected nitrate measurements following persulfate oxidation by the cleaned sample mass. Small sample sizes preclude duplicate CRS samples, but duplicate measurements of vegetative samples yield 0.4‰ analytical precision of  $\delta^{15}\text{N}_{\text{DB}}$  measurements.

## 3. Results

### 3.1. Sedimentary CRS Abundance and $\delta^{15}\text{N}_{\text{DB}}$

CRS are more abundant in spring laminae, with an average relative abundance of  $87\% \pm 6\%$ , compared to  $74\% \pm 7\%$  in summer laminae. Similarly, relative surface area averages  $81\% \pm 6\%$  and  $61\% \pm 12\%$  in spring and summer laminae, respectively (Table 1).

The average  $\delta^{15}\text{N}_{\text{DB}}$  value for the entire <63  $\mu\text{m}$  diatom community ( $\delta^{15}\text{N}_{\text{DB-bulk}}$ ) is  $9.0 \pm 0.7\text{‰}$ , while the average  $\delta^{15}\text{N}_{\text{DB}}$  value for the isolated *Chaetoceros* ( $\delta^{15}\text{N}_{\text{DB-Ch}}$ ) is  $7.8 \pm 0.6\text{‰}$  (Figure 3). According to a Wilcoxon signed rank test,  $\delta^{15}\text{N}_{\text{DB-Ch}}$  values are statistically significantly lower than  $\delta^{15}\text{N}_{\text{DB-bulk}}$  values ( $p = 0.0029$ ).

Seasonally,  $\delta^{15}\text{N}_{\text{DB}}$  values tend to be lower in summer laminae (Figure 3). Wilcoxon rank sum tests reveal that summer  $\delta^{15}\text{N}_{\text{DB-bulk}}$  and  $\delta^{15}\text{N}_{\text{DB-Ch}}$  values are statistically significantly lower than spring values ( $p = 0.0096$  and  $p = 0.0025$ , respectively). The offset between  $\delta^{15}\text{N}_{\text{DB-bulk}}$  and  $\delta^{15}\text{N}_{\text{DB-Ch}}$  ( $\delta^{15}\text{N}_{\text{DB-offset}} = \delta^{15}\text{N}_{\text{DB-bulk}} - \delta^{15}\text{N}_{\text{DB-Ch}}$ ) is significantly less in the CRS-dominated spring laminae versus summer laminae ( $p = 0.0081$ ).

### 3.2. Culture Growth, Spore Formation, Nutrient Utilization, and Silicification

Due to insufficient separation of CRS from vegetative frustules following the first two experiments, the data presented below derive from the third experiment, unless otherwise noted. Data from the first two experiments are archived at the U.S. Antarctic Program Data Center (Dove, 2023a).

Experiment 3 cultures grew exponentially until day 6, when vegetative cells were harvested (Figure 2). Fluorescence decreased following nitrate depletion and the onset of resting spore formation. Resting spores first appeared on day 7 in carboys 1 and 3 and on day 6 in carboy 2. Spore formation continued until harvesting on day 36, with approximately 17% of cells sporulating (Table 2).

**Table 1**  
Seasonal Diatom Assemblage and Geochemical Data From ODP Core 1098B-5H-7 Deglacial Sediments

Depth (cm)	Season	$\delta^{15}\text{N}_{\text{DB-bulk}}$ (‰)	Bulk N:Si	$\delta^{15}\text{N}_{\text{DB-Ch}}$ (‰)	Ch. N:Si	$\delta^{15}\text{N}_{\text{DB-offset}}$ (‰)	%CRS (count)	%CRS (surface area)	Calc. $\delta^{15}\text{N}_{\text{DB-other}}$ (‰)
12–14.5	Spring	9.3	24.0	9.2	19.9	0.1	95	89	10.1
15–18	Spring	9.8	15.8	9.5	15.0	0.3	91	83	11.3
18–19.5	Summer	8.6	11.0	7.4	15.5	1.2	78	71	11.5
23–25.5	Summer	7.6	22.8	6.6	23.4	1.0	81	70	9.9
25.5–27	Spring	10.3	14.8	9.1	14.7	1.2	87	78	14.4
27.5–31	Spring	9.2	18.2	9.3	17.1	−0.1	85	83	8.7
32–35.5	Summer	8.6	18.8	5.9	22.2	2.7	76	60	12.7
36.5–40	Summer	8.8	26.2	6.8	17.1	2.0	74	67	12.9
44.5–47	Spring	8.9	26.0	7.9	17.5	1.0	83	74	11.8
53–54.5	Summer	8.9	22.3	6.4	16.1	2.5	72	61	12.9
55–60	Summer	9.0	22.7	6.0	17.9	3.0	60	40	11.0
63.5–65.5	Spring	8.9	22.4	8.9	19.8	0	79	77	8.9

Note.  $\delta^{15}\text{N}_{\text{DB-bulk}}$  describes the measurements from the entire <63  $\mu\text{m}$  diatom community,  $\delta^{15}\text{N}_{\text{DB-Ch}}$  describes the measurements from isolated *Chaetoceros*, and  $\delta^{15}\text{N}_{\text{DB-offset}} = \delta^{15}\text{N}_{\text{DB-bulk}} - \delta^{15}\text{N}_{\text{DB-Ch}}$ . N:Si ratios are reported for the bulk community and *Chaetoceros* samples as  $\mu\text{mol N}$  per gram of biogenic silica.  $\delta^{15}\text{N}_{\text{DB-other}}$  is the calculated value of non-CRS diatoms.

Average initial nitrate concentrations were  $44.7 \pm 3.4 \mu\text{M}$  with an average  $\delta^{15}\text{N}_{\text{NO}_3}$  of  $9.6 \pm 0.4\text{‰}$ . Nitrate was fully depleted by day 5 and  $\delta^{15}\text{N}_{\text{NO}_3}$  values increased with progressive consumption (Figure 2). Ammonium concentration was initially  $2.3 \pm 0.7 \mu\text{M}$  and fully depleted by day 4. Concentrations then increased and oscillated between  $\sim 1$  and  $3 \mu\text{M}$  throughout the remainder of the experiment (Figure 2). Total reduced N concentrations oscillate between  $\sim 30$  and  $50 \mu\text{M}$  (Figure S3 in Supporting Information S1), with  $\delta^{15}\text{N}$  values ranging between  $-2$  and  $3\text{‰}$  (Figure 2).

The dSi concentrations initially averaged  $40.7 \pm 1.4 \mu\text{M}$  and decreased to full depletion by day 11 (Figure 2). When vegetative cells were harvested on day 6, just prior to sporulation, dSi concentrations averaged  $30.6 \pm 1.1 \mu\text{M}$ . dSi utilization along with cell counts enabled calculation of cellular silicification (Table 2). *Chaetoceros* cells—CRS and remnant vegetative frustules—were more heavily silicified at the end of the experiment. In addition to being more heavily silicified, isolated CRS have a higher N:Si ratio than vegetative cells, although the difference is not statistically significant ( $p = 0.069$ ).

### 3.3. Culture $\delta^{15}\text{N}_{\text{biomass}}$ , $\delta^{15}\text{N}_{\text{DB}}$ , and $\epsilon_{\text{DB}}$

Average  $\delta^{15}\text{N}_{\text{biomass}}$  is  $8.0 \pm 0.8\text{‰}$  for harvested vegetative cells and  $6.7 \pm 1.0\text{‰}$  for mixed vegetative cells and CRS (Figure 4a). Since the carboys contained dead vegetative cells in addition to CRS, it is impossible to measure the  $\delta^{15}\text{N}$  of biomass exclusively from CRS. The average  $\delta^{15}\text{N}_{\text{biomass}}$  value of  $8.0 \pm 0.8\text{‰}$  for harvested vegetative cells meets expectations given that all nitrate with an initial  $\delta^{15}\text{N}_{\text{NO}_3}$  value of  $9.6 \pm 0.4\text{‰}$ , plus some amount of reduced N with a low  $\delta^{15}\text{N}$  value, is consumed.

Average  $\delta^{15}\text{N}_{\text{DB}}$  for vegetative *Chaetoceros* is  $6.5 \pm 1.7\text{‰}$ . The  $\delta^{15}\text{N}_{\text{DB}}$  value from carboy 2, in which CRS formation had already begun at the time of harvesting, is approximately  $3\text{‰}$  lower than the values from carboys 1 and 3, which together average  $7.5 \pm 0.3\text{‰}$ . The  $\delta^{15}\text{N}_{\text{DB}}$  values for CRS in carboys 2 and 3 are  $-2.8 \pm 0.4\text{‰}$  and  $-0.5 \pm 0.4\text{‰}$ , respectively (Figure 4c). No  $\delta^{15}\text{N}_{\text{DB}}$  value was measured from carboy 1 due to insufficient sample size following CRS isolation.

Across all experiments and adjusted to a single initial  $\delta^{15}\text{N}_{\text{NO}_3}$  value, average  $\delta^{15}\text{N}_{\text{DB}}$  values for vegetative *Chaetoceros* is  $10.0 \pm 2.2\text{‰}$ . Mixed vegetative and CRS samples from the first two experiments and from carboy 2 of the third experiment have an average  $\delta^{15}\text{N}_{\text{DB}}$  value of  $8.9 \pm 2.9\text{‰}$ .

The calculated  $\epsilon_{\text{DB}}$  value ( $\delta^{15}\text{N}_{\text{biomass}} - \delta^{15}\text{N}_{\text{DB}}$ ) for vegetative *Chaetoceros* in the third experiment is  $0.4 \pm 1.4\text{‰}$ , excluding the sample from carboy 2 that contains CRS, while the calculated  $\epsilon_{\text{DB}}$  value for vegetative

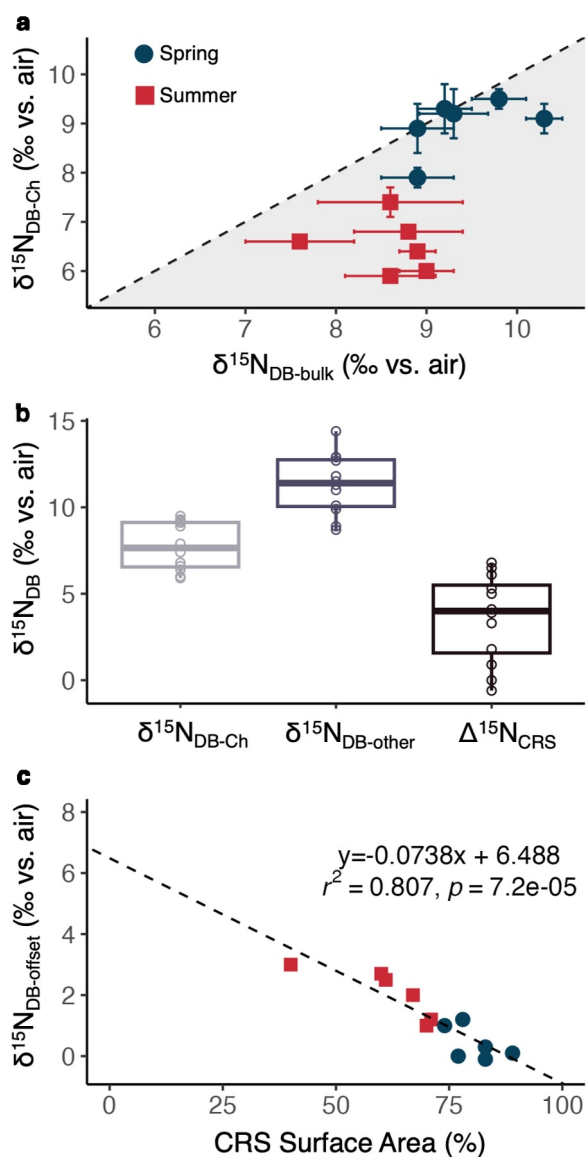


**Figure 3.**  $\delta^{15}\text{N}_{\text{DB}}$  measurements and calculated CRS-related isotopic offsets from ODP Site 1098 sediments. Panel (a) plots  $\delta^{15}\text{N}_{\text{DB}}$  measured from the entire  $<63\ \mu\text{m}$  diatom community ( $\delta^{15}\text{N}_{\text{DB-bulk}}$ ) against isolated *Chaetoceros* ( $\delta^{15}\text{N}_{\text{DB-Ch}}$ ), with blue circles representing spring laminae and red squares representing summer laminae. The gray shaded region represents  $\delta^{15}\text{N}_{\text{DB-Ch}}$  values lower than  $\delta^{15}\text{N}_{\text{DB-bulk}}$  values. Panel (b) shows boxplots of  $\delta^{15}\text{N}_{\text{DB-Ch}}$ , calculated non-CRS  $\delta^{15}\text{N}_{\text{DB}}$  values ( $\delta^{15}\text{N}_{\text{DB-other}}$ ), and the difference between them ( $\Delta\delta^{15}\text{N}_{\text{CRS}}$ ). Calculations are described in Section 4.3. Panel (c) shows a linear regression of the isotopic offset between  $\delta^{15}\text{N}_{\text{DB-bulk}}$  and  $\delta^{15}\text{N}_{\text{DB-Ch}}$  ( $\delta^{15}\text{N}_{\text{DB-offset}}$ ) as a function of CRS surface area contribution (%CRS<sub>SA</sub>). The y-intercept represents an estimate of  $\Delta\delta^{15}\text{N}_{\text{CRS}}$ .

#### 4.2. Seasonal $\delta^{15}\text{N}_{\text{DB}}$ Signal

Statistically significant differences in both  $\delta^{15}\text{N}_{\text{DB-Ch}}$  and  $\delta^{15}\text{N}_{\text{DB-offset}}$  in spring versus summer laminae indicate that  $\delta^{15}\text{N}_{\text{DB}}$  values are impacted by seasonal effects (Figure 3). The smaller offset between  $\delta^{15}\text{N}_{\text{DB-bulk}}$  and  $\delta^{15}\text{N}_{\text{DB-Ch}}$  in spring laminae can partially be explained by the bulk diatom assemblage being dominated by CRS, but the inter-seasonal differences in  $\delta^{15}\text{N}_{\text{DB-Ch}}$  warrant further investigation.

*Chaetoceros* across all experiments is  $-1.5 \pm 2.6\text{‰}$ . In contrast to vegetative *Chaetoceros*, CRS are characterized by an anomalously high  $\epsilon_{\text{DB}}$  value of  $8.0 \pm 2.7\text{‰}$  (Figure 4d).

#### 4. Discussion

Both sedimentary data and laboratory culture experiments suggest that CRS are characterized by low  $\delta^{15}\text{N}_{\text{DB}}$  values and, consequently, high  $\epsilon_{\text{DB}}$  values relative to vegetative *Chaetoceros* and other diatoms. While Horn, Robinson, et al. (2011) found  $\epsilon_{\text{DB}}$  values up to 11.2‰ in monospecific diatom cultures, additional culture studies (Jones et al., 2022) and fieldwork (Morales et al., 2014; Robinson et al., 2020) show consistently negative  $\epsilon_{\text{DB}}$  values for diatom communities. A discussion of potential explanations for the incongruously high  $\epsilon_{\text{DB}}$  values of Horn, Robinson, et al. (2011) is found in Jones et al. (2022). The calculated average  $\epsilon_{\text{DB}}$  value of  $-1.5 \pm 2.6\text{‰}$  for vegetative *Chaetoceros* is consistent with modern field observations ( $-3.2 \pm 1.5\text{‰}$ ; Robinson et al., 2020) and experimental results ( $-4.8 \pm 0.8\text{‰}$ ; Jones et al., 2022). Possible explanations for low CRS-specific  $\delta^{15}\text{N}_{\text{DB}}$  values and impact on paleo records are explained below.

##### 4.1. Differences in Culture Versus Sediment $\delta^{15}\text{N}_{\text{DB}}$ Measurements

While low CRS-specific  $\delta^{15}\text{N}_{\text{DB}}$  values are consistent between culture and sediment, CRS-specific  $\delta^{15}\text{N}_{\text{DB}}$  measurements range from approximately  $-1\text{‰}$  in culture to approximately 9‰ in sediments. Since differences in CRS-specific  $\delta^{15}\text{N}_{\text{DB}}$  absolute values are expected due to variation in source  $\delta^{15}\text{N}_{\text{NO}_3}$ , we focus on the relationship between  $\delta^{15}\text{N}_{\text{DB}}$  values in CRS and non-CRS diatoms ( $\Delta\delta^{15}\text{N}_{\text{CRS}}$ ). For sediment samples,  $\Delta\delta^{15}\text{N}_{\text{CRS}}$  is calculated by subtracting  $\delta^{15}\text{N}_{\text{DB-Ch}}$  from  $\delta^{15}\text{N}_{\text{DB-other}}$ . For culture samples,  $\Delta\delta^{15}\text{N}_{\text{CRS}}$  is quantified by subtracting the  $\delta^{15}\text{N}_{\text{DB}}$  value of CRS from the  $\delta^{15}\text{N}_{\text{DB}}$  value of vegetative counterparts.

We also recognize that culture conditions likely impacted  $\delta^{15}\text{N}_{\text{DB}}$  values. There are many examples of differing physiological responses within culture to variable nutrient-nitrogen availability (Eppley & Renger, 1974; Yodsuwan et al., 2017), dissolved silica concentrations (Penna et al., 2003), and light conditions (Brzezinski, 1985; Saito & Tsuda, 2003). While the N and dSi depletion observed at the end of our culture experiments is feasibly reflective of late-season conditions in the Southern Ocean, particularly in highly productive coastal regions, the initial nitrate and dSi concentrations differ from those typical of the Southern Ocean surface. Our initial nitrate concentrations of  $\sim 45\ \mu\text{M}$  exceed while initial dSi concentrations of  $\sim 40\ \mu\text{M}$  fall below average surface conditions (Reagan et al., 2024). Consistency with sedimentary results corroborates the overall trend of CRS recording lower  $\delta^{15}\text{N}_{\text{DB}}$  values than vegetative *Chaetoceros*, but specific values of  $\delta^{15}\text{N}_{\text{DB}}$  measurements,  $\epsilon_{\text{DB}}$  calculations, and cellular stoichiometry are likely products of culture conditions. We therefore focus on sedimentary data for quantitative assessments of CRS impact on sedimentary  $\delta^{15}\text{N}_{\text{DB}}$  records.

**Table 2**  
Cell Counts, N:Si Ratio Reported as  $\mu\text{mol N per Gram of Biogenic Silica (bSi)}$ , and Calculated Cellular Silicification From the Third Culture Experiment

	Cells/L	CRS/L	%CRS	$\mu\text{mol N: g bSi}$	pmol Si/cell
C1 veg. harvest	$7.4 \times 10^7$	0	0	17.6	0.14
C2 veg. harvest	$7.3 \times 10^7$	$2.9 \times 10^6$	3.9	18.1	0.10
C3 veg. harvest	$1.1 \times 10^8$	0	0	16.4	0.12
C1 CRS harvest	$4.2 \times 10^7$	$7.4 \times 10^6$	17.4	–	0.89
C2 CRS harvest	$4.8 \times 10^7$	$8.5 \times 10^6$	17.9	24.1	0.78
C3 CRS harvest	$3.7 \times 10^7$	$6.1 \times 10^6$	16.8	18.5	1.11

The nearly monogenic layers of CRS within ODP Site 1098 are interpreted to represent a spring bloom that rapidly depleted nutrients within a stratified water column, while open water diatom species in summer laminae suggest ice-free conditions and a less stratified water column (Maddison et al., 2005). Higher  $\delta^{15}\text{N}_{\text{DB-bulk}}$  and  $\delta^{15}\text{N}_{\text{DB-Ch}}$  values are expected in the spring due to near-complete nutrient utilization. Another potential

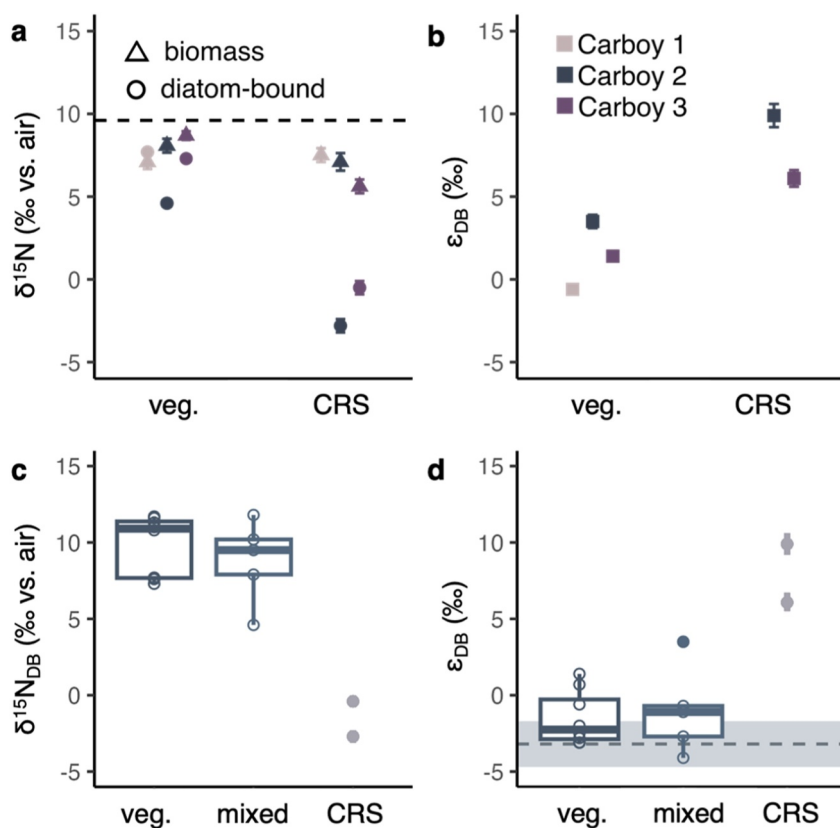


**Figure 4.** Isotope measurements and  $\epsilon_{\text{DB}}$  calculations from culture experiments. Panels (a) and (b) show data from experiment 3, color-coded by carboy, while panels (c) and (d) show data from all experiments, with  $\delta^{15}\text{N}_{\text{DB}}$  values normalized to account for changes in initial  $\delta^{15}\text{N}_{\text{NO}_3}$  between experiments. The nitrogen isotopic composition of vegetative *Chaetoceros* frustules is enriched in  $^{15}\text{N}$  relative to CRS (a). The dotted black line denotes the average initial  $\delta^{15}\text{N}_{\text{NO}_3}$  value of 9.6‰. Circles represent  $\delta^{15}\text{N}_{\text{DB}}$  measurements and triangles represent  $\delta^{15}\text{N}_{\text{biomass}}$  measurements. These measurements are used to calculate the  $\epsilon_{\text{DB}}$  values ( $\delta^{15}\text{N}_{\text{biomass}} - \delta^{15}\text{N}_{\text{DB}}$ ) shown in panel (b).  $\delta^{15}\text{N}_{\text{DB}}$  measurements (c) and  $\epsilon_{\text{DB}}$  calculations (d) for vegetative cells from all experiments ( $n = 8$ ) and mixed samples from the first two experiments plus carboy 2 of experiment 3 ( $n = 5$ ) are presented as boxplots.  $\delta^{15}\text{N}_{\text{DB}}$  values from all experiments are adjusted to a single initial  $\delta^{15}\text{N}_{\text{NO}_3}$  value. CRS  $\delta^{15}\text{N}_{\text{DB}}$  and  $\epsilon_{\text{DB}}$  values are plotted as points because CRS are successfully isolated from two carboys during experiment 3. The dotted gray line and gray shading indicate average  $\epsilon_{\text{DB}}$  ( $-3.2 \pm 1.5\text{‰}$ ) in the Antarctic Zone of the Southern Ocean (Robinson et al., 2020). CRS  $\epsilon_{\text{DB}}$  is higher than that of vegetative *Chaetoceros* and  $\epsilon_{\text{DB}}$  measured in the field (d).

explanation for higher  $\delta^{15}\text{N}_{\text{DB}}$  in spring samples is high- $\delta^{15}\text{N}$  nitrate from melting sea ice, as  $\delta^{15}\text{N}$  values up to 8.1‰ have been measured in Antarctic sea ice (Fripiat et al., 2014). Lower  $\delta^{15}\text{N}_{\text{DB-bulk}}$  and  $\delta^{15}\text{N}_{\text{DB-Ch}}$  values in the summer are likely due to decreased nutrient utilization and possibly assimilation of low- $\delta^{15}\text{N}$  ammonium, as field data suggest that ammonium assimilation by diatoms late in the open ocean growing season results in lower  $\delta^{15}\text{N}_{\text{DB}}$  (Robinson et al., 2020). This interpretation is supported by increasing ammonium concentrations throughout the modern growing season on the western Antarctic Peninsula (Henley et al., 2017). Beyond seasonal differences in nutrient availability, the large  $\delta^{15}\text{N}_{\text{DB-offset}}$  in summer laminae may be related to seasonal changes in temperature or light period and intensity. Such environmentally driven internal N isotope systematic effects are further discussed in Section 4.4.3.

### 4.3. $\delta^{15}\text{N}_{\text{DB}}$ Differences Between CRS and Non-CRS Diatoms

Culture and sedimentary data inform semi-quantitative differences between  $\delta^{15}\text{N}_{\text{DB}}$  values of CRS and other diatoms. The difference between cultured vegetative *Chaetoceros* and CRS  $\delta^{15}\text{N}_{\text{DB}}$  values is first quantified using data from experiment 3. The  $\delta^{15}\text{N}_{\text{DB}}$  values of the two successfully isolated CRS samples are on average  $7.7 \pm 0.5\text{‰}$  lower than their mostly vegetative counterparts (Figure 4). Prior to calculating this difference for carboy 2, the vegetative  $\delta^{15}\text{N}_{\text{DB}}$  measurement was corrected from  $4.6 \pm 0.2\text{‰}$  to  $4.9 \pm 0.5\text{‰}$ , to account for the 4% of cells that had sporulated. To do so, we assume a  $\delta^{15}\text{N}_{\text{DB}}$  value of  $-2.8 \pm 0.4\text{‰}$  for the CRS based on the CRS-specific  $\delta^{15}\text{N}_{\text{DB}}$  measurement from carboy 2. An average  $\Delta\delta^{15}\text{N}_{\text{CRS}}$  value of  $7.7 \pm 0.5\text{‰}$  is consistent with data from other experiments, as a mass balance calculation using average vegetative and mixed sample  $\delta^{15}\text{N}_{\text{DB}}$  values from the first two experiments (see SI), assuming that 17% of cells in mixed samples are resting spores, yields a  $\Delta\delta^{15}\text{N}_{\text{CRS}}$  value, or difference between vegetative  $\delta^{15}\text{N}_{\text{DB}}$  and CRS  $\delta^{15}\text{N}_{\text{DB}}$ , of  $6.3 \pm 3.7\text{‰}$ .

Sedimentary data yield results consistent with the culture data while removing potential bias introduced from culture conditions that are not representative of the Southern Ocean environment. To isolate a  $\delta^{15}\text{N}_{\text{DB}}$  value of non-*Chaetoceros* diatoms from the measured bulk sediment  $\delta^{15}\text{N}_{\text{DB-bulk}}$  value, we conduct a simple mass balance calculation (Equation 1), quantifying CRS contribution by their relative surface area (%CRS<sub>SA</sub>).

$$\delta^{15}\text{N}_{\text{DB-bulk}} = \delta^{15}\text{N}_{\text{DB-Ch}} * (\% \text{CRS}_{\text{SA}}) + \delta^{15}\text{N}_{\text{DB-other}} * (1 - \% \text{CRS}_{\text{SA}}) \quad (1)$$

Although vegetative *Chaetoceros* are present in the isolated samples and thus potentially influence assessments of CRS-specific  $\delta^{15}\text{N}_{\text{DB}}$  values, we consider these effects negligible due to their lower degree of silicification and lower N:Si ratio (Table 2). Additionally, our discrete diatom counts indicate that CRS comprise on average over 80% of the *Chaetoceros* community. Between the 12 samples, our mass balance calculation reveals that average calculated  $\delta^{15}\text{N}_{\text{DB-other}}$  is  $11.3 \pm 1.7\text{‰}$ , resulting in an average difference ( $\delta^{15}\text{N}_{\text{DB-other}} - \delta^{15}\text{N}_{\text{DB-Ch}} = \Delta\delta^{15}\text{N}_{\text{CRS}}$ ) of  $3.6 \pm 2.5\text{‰}$  (Table 1, Figure 3b).

An additional estimate of  $\Delta\delta^{15}\text{N}_{\text{CRS}}$  is calculated with a linear regression of  $\delta^{15}\text{N}_{\text{DB-offset}}$  as a function of %CRS<sub>SA</sub>. Assuming that the relationship is linear, the y-intercept yields the expected  $\delta^{15}\text{N}_{\text{DB-offset}}$  value in a sample with no CRS present, therefore providing an estimate of the difference between  $\delta^{15}\text{N}_{\text{DB-other}}$  and  $\delta^{15}\text{N}_{\text{DB-Ch}}$ . According to the linear regression,  $\Delta\delta^{15}\text{N}_{\text{CRS}}$  is  $6.5 \pm 1.3\text{‰}$  (Figure 3c), meaning CRS record  $\delta^{15}\text{N}_{\text{DB}}$  values approximately 6.5‰ lower than other diatoms in marine sediment.

We note that %CRS<sub>SA</sub> does not fully constrain the relative amount of organic N that CRS contribute to the bulk diatom assemblage N pool because of varying N:Si ratios from the bulk community versus isolated *Chaetoceros* samples (Table 1). While frustule N content would provide the ideal parameter for our mass balance calculation and linear regression, we are unable to constrain frustule N content in the absence of cellular silicification measurements. We opt to use %CRS<sub>SA</sub> measurements rather than calculations of N content from N:Si measurements requiring assumptions about cellular silicification, as previous work has shown that cellular silicification can range nearly an order of magnitude within the same genus (McNair et al., 2018).

### 4.4. Reasons for Low CRS $\delta^{15}\text{N}_{\text{DB}}$ Values

Our results are surprising given that CRS form under nutrient depleted conditions, when one would expect high  $\delta^{15}\text{N}_{\text{DB}}$  values reflective of high  $\delta^{15}\text{N}_{\text{NO}_3}$  in the absence of internal fractionation processes. Nevertheless,  $\Delta\delta^{15}\text{N}_{\text{CRS}}$  values are comparable between cultures (2.6–8.2‰) and sediment (1.1–7.8‰). We identify three

possible explanations for why CRS record low  $\delta^{15}\text{N}_{\text{DB}}$  values relative to vegetative *Chaetoceros* and to other diatoms: ammonium assimilation, silicification, and internal N allocation during sporulation.

#### 4.4.1. Assimilation of Reduced Nitrogen

Lower  $\delta^{15}\text{N}_{\text{biomass}}$  values observed after resting spore formation in the experiment suggest assimilation of isotopically light N, likely ammonium or other bioavailable reduced N. Observed increases in reduced N concentration throughout the experiment are likely due to remineralization by bacteria since the cultures are not axenic, while decreases are due to consumption by both diatoms and bacteria. Although bacterial nutrient consumption is not quantified, we assume that it minimally influences interpretations because the majority of nutrient-nitrogen is nitrate consumed by diatoms.

Southern Ocean field observations from late in the diatom growing season suggest that assimilation of regenerated ammonium results in low particulate and diatom-bound  $\delta^{15}\text{N}$  values (Robinson et al., 2020). Ammonium concentrations measured throughout the culture experiment suggest that ammonium, either regenerated or pre-existing in culture media, is consumed prior to and during CRS formation (Figure 2). Given consistently low  $\delta^{15}\text{N}$  values for total reduced N, ammonium assimilation could lead to lower  $\delta^{15}\text{N}_{\text{DB}}$  values in CRS.

While ammonium, or another form of bioavailable reduced N such as urea, likely contributed to lower  $\delta^{15}\text{N}_{\text{DB}}$  values in culture, it does not fully account for the large difference between CRS and vegetative cells. Conservatively estimating that all reduced N consumed has a  $\delta^{15}\text{N}$  value of 0‰, it would not be possible for assimilation alone to explain the average observed  $\delta^{15}\text{N}_{\text{DB}}$  value of  $-1.6\text{‰}$  for CRS (SI Equation 1).

#### 4.4.2. Silicification

Although no research into CRS silicification has presently been published, past work on silicification using the model species *Thalassiosira pseudonana* shows that genes involved in silicification are upregulated at times when frustule structures are not being made (Kotzsch et al., 2017; Tesson et al., 2017). The implication that proteins are synthesized before they are needed suggests that the N-containing structures necessary for sporulation could be synthesized prior to nutrient depletion, when  $^{14}\text{N}$  is more abundant. If this is the case, the N bound within CRS could have inherited its low  $\delta^{15}\text{N}$  value from dissolved nutrients early in the growing season.

Previous culture work suggests an association between silicification and  $\epsilon_{\text{DB}}$ . Robinson et al. (2025) found that one species grown in culture, *Fragilariopsis rhombica*, had a low N:Si uptake ratio and a positive  $\epsilon_{\text{DB}}$  value, suggesting a relationship between silicification and  $\delta^{15}\text{N}_{\text{DB}}$  values. Since CRS are more heavily silicified than vegetative *Chaetoceros*, silicification could be an important driver of low  $\delta^{15}\text{N}_{\text{DB}}$  in CRS. Still, further research is necessary to characterize the N:Si relationship in different species and to identify the mechanism behind this relationship.

#### 4.4.3. Internal N Allocation

With similar  $\delta^{15}\text{N}_{\text{biomass}}$  values between vegetative *Chaetoceros* and CRS, low  $\delta^{15}\text{N}_{\text{DB}}$  values in CRS consequently lead to high calculated  $\epsilon_{\text{DB}}$  values. Although our CRS-specific  $\epsilon_{\text{DB}}$  calculations are affected by biomass accumulated from vegetative *Chaetoceros*, the large difference between  $\delta^{15}\text{N}_{\text{biomass}}$  and CRS  $\delta^{15}\text{N}_{\text{DB}}$  points to internal processes that greatly favor incorporation of  $^{14}\text{N}$  into resting spore frustules.

While our work does not provide an answer as to why CRS display strong allocation of  $^{14}\text{N}$  to resting spore frustules, our data show a clear trend of CRS recording low  $\delta^{15}\text{N}_{\text{DB}}$  values that warrants speculation and future investigation. The observed seasonal differences in  $\delta^{15}\text{N}_{\text{DB-offset}}$  as well as variable  $\epsilon_{\text{DB}}$  values under different light conditions in culture (Horn, Robinson, et al., 2011; Jones et al., 2022) suggests that light intensity and duration potentially impacts internal N isotope fractionation in both CRS and other diatom species. Production of the amino acid serine, which is abundant among frustule-bound proteins (Bromke, 2013) is synthesized in part by the photorespiration pathway in plants (Zimmermann et al., 2021), providing a possible mechanistic relationship between light and internal N isotope fractionation. Another potential environmental driver of low  $\delta^{15}\text{N}_{\text{DB}}$  values in CRS is seasonal differences in nutrient-N availability. In terms of biosynthetic pathways, diatoms' unique ability to utilize the urea cycle could contribute to CRS recording low  $\delta^{15}\text{N}_{\text{DB}}$  values when nitrate-limited (Allen et al., 2011; Kröger & Poulsen, 2008). Finally, we also speculate the possibility of recycled chlorophyll providing an internal source of low- $\delta^{15}\text{N}$  nitrogen during resting spore formation (Werner & Schmidt, 2002).

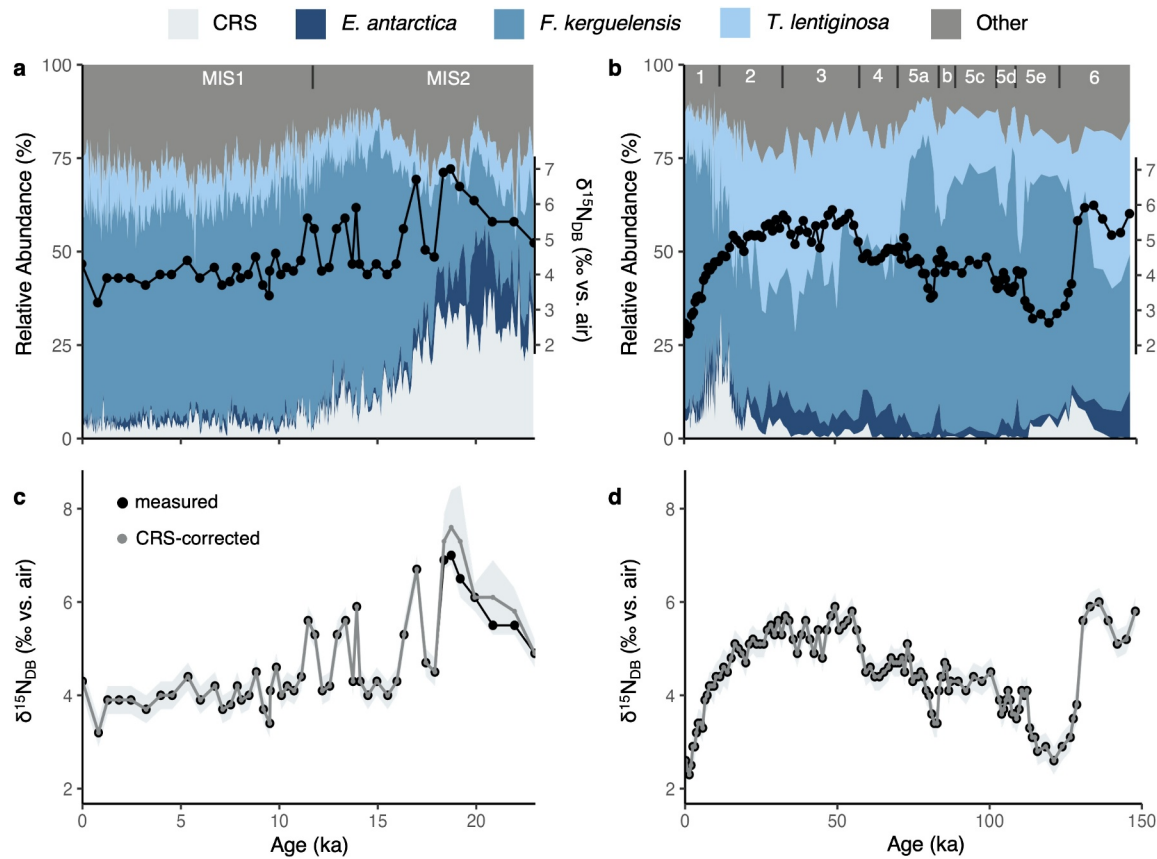


**Figure 5.** Diatom assemblage data,  $\delta^{15}\text{N}_{\text{DB}}$  records from sediment cores TN057-13-PC4 and MD11-3353, and CRS-corrected  $\delta^{15}\text{N}_{\text{DB}}$  records. Panels (a) and (b) show  $\delta^{15}\text{N}_{\text{DB}}$  (black line) and relative abundance of select diatom species (colored shading) throughout TN057-13-PC4 and MD11-3353, respectively. Panels (c) and (d) show CRS-corrected  $\delta^{15}\text{N}_{\text{DB}}$  data and propagated uncertainty (gray line and shading) plotted over measured  $\delta^{15}\text{N}_{\text{DB}}$  (black line) from the same cores. TN057-13-PC4  $\delta^{15}\text{N}_{\text{DB}}$  data from Horn, Beucher, et al. (2011) and diatom data from Nielsen (2004). MD11-3353  $\delta^{15}\text{N}_{\text{DB}}$  data from Ai et al. (2020) and diatom data from Civel-Mazens et al. (2021).

#### 4.5. Paleoceanographic Implications

Since CRS can comprise a significant proportion of sedimentary diatom assemblages in the Southern Ocean (Armand et al., 2005; Crosta et al., 1997; Esper et al., 2010; Zielinski & Gersonde, 1997), their unique N isotopic signature must be considered when applying the  $\delta^{15}\text{N}_{\text{DB}}$  proxy to paleoceanographic research, particularly quantitative reconstructions (e.g., Kemeny et al., 2018). A pertinent case study is that of glacial-interglacial cycles, wherein  $\delta^{15}\text{N}_{\text{DB}}$  values tend to increase during glacial periods (Ai et al., 2020; Robinson et al., 2004, 2005; Studer et al., 2015) and CRS tend to become more abundant in sediments underlying the modern Polar Front due to increased northward sea ice extent (Abelmann et al., 2006). Considering glacial-interglacial shifts in diatom assemblage is important because increased CRS abundance during glacial periods could potentially bias  $\delta^{15}\text{N}_{\text{DB}}$  measurements toward lower values and therefore lead to underestimates of the biological pump's role in lowering glacial atmospheric  $\text{CO}_2$ .

Diatom assemblage data and  $\delta^{15}\text{N}_{\text{DB}}$  measurements spanning at least one glacial-interglacial cycle are available from sediment cores TN057-13-PC4 and MD11-3353, which are respectively located in the Antarctic Zone of the Atlantic sector and offshore of subantarctic islands in the Polar Frontal Zone of the Indian sector of the Southern Ocean (Figure 1). The  $\delta^{15}\text{N}_{\text{DB}}$  record from TN057-13-PC4, which spans  $\sim 23$  ka to present, is unique in that interglacial values are higher than glacial values (Horn, Beucher, et al., 2011). The CRS relative abundance is consistently below 10% during the Holocene and reaches a maximum of  $\sim 40\%$  during the last glacial period (Nielsen, 2004; Figure 5a). In the 150-kyr MD11-3353 record, glacial  $\delta^{15}\text{N}_{\text{DB}}$  values are approximately 4‰ higher than interglacial values (Ai et al., 2020) and CRS relative abundance peaks around 30% following the most recent deglaciation  $\sim 12$  ka, with a smaller CRS peak occurring  $\sim 130$  ka (Civel-Mazens et al., 2021; Figure 5b).

The deglacial timing of maximum CRS relative abundance is related to the core's proximity to subantarctic islands, as increased nutrient-rich runoff likely stimulated *Chaetoceros* production. Other climatically relevant species (Abelmann et al., 2006; Jacot Des Combes et al., 2008) present throughout both records include *Eucampia antarctica*, *Fragilariopsis kerguelensis*, and *Thalassiosira lentiginosa* (Figure 5).

To assess how diatom assemblage impacts these  $\delta^{15}\text{N}_{\text{DB}}$  records, we first convert CRS relative abundance to relative surface area contribution with the linear relationship revealed by data collected from ODP Site 1098 (Table 1, Figure S4 in Supporting Information S1). Due to the small size of CRS, relative abundances below approximately 28% equate to negligible surface area contribution. Recognizing that CRS size, and therefore surface area contribution, may not be consistent in sediments from the coastal Antarctic versus the open ocean due to different community composition and particularly lower CRS relative abundance, we propagate an uncertainty of  $\pm 10\%$  CRS surface area contribution.

We then use the linear relationship between CRS surface area contribution and  $\delta^{15}\text{N}_{\text{DB-offset}}$  to calculate the expected isotopic bias due to variable CRS abundance. For example, taking the maximum CRS relative abundance of 33% in MD11-3353, or 7% surface area contribution, we calculate an expected  $\delta^{15}\text{N}_{\text{DB-offset}}$  of 6.0‰. Since the expected  $\delta^{15}\text{N}_{\text{DB}}$  in a sample without significant CRS surface area contribution is 6.5‰, the 7% increase in surface area contribution results in an expected  $\delta^{15}\text{N}_{\text{DB}}$  bias of 0.5‰ (6.5–6.0‰). In other words, in a sample with a CRS relative abundance of 33%, the  $\delta^{15}\text{N}_{\text{DB}}$  measurement is expected to be 0.5‰ lower because of the CRS (Figure S5 in Supporting Information S1). An important caveat is that our assessment of CRS bias to open ocean  $\delta^{15}\text{N}_{\text{DB}}$  records relies upon the assumption of a consistent relationship between CRS relative abundance and surface area contribution as well as consistency between surface area and N contribution well outside of the range of data used to establish the relationship. Tighter constraint on CRS effect on  $\delta^{15}\text{N}_{\text{DB}}$  records can be achieved through future work that quantifies both genus- or species-specific surface area contribution or, better yet, N:Si and cellular silicification.

Our calculations of CRS-corrected  $\delta^{15}\text{N}_{\text{DB}}$  throughout TN057-13-PC4 and MD11-3353 reveal that the long-term trends in  $\delta^{15}\text{N}_{\text{DB}}$  do not meaningfully change across glacial-interglacial cycles (Figure 5). Given that the calculation was performed using a high-end estimate of  $\Delta\delta^{15}\text{N}_{\text{CRS}}$ , the theoretical assemblage-specific effects on  $\delta^{15}\text{N}_{\text{DB}}$  records are likely negligible in most cases. Although CRS relative abundance increases by nearly 30% in TN057-13-PC4 during the glacial period, CRS relative contribution to total diatom surface area increases by only about 6% due to the small size of CRS compared to other diatoms such as *T. lentiginosa*.

While long-term  $\delta^{15}\text{N}_{\text{DB}}$  trends appear unaffected by variable CRS relative abundance, individual datapoints throughout the TN057-13-PC4 record change as much as  $0.8 \pm 1.2\text{‰}$  with an 11% increase in CRS surface area contribution. We therefore urge caution and when applying  $\delta^{15}\text{N}_{\text{DB}}$  records to quantitative analyses when there are perceptible changes in CRS relative abundance. Based on our data and typical measurement precision of  $\sim 0.3\text{‰}$ , shifts in CRS relative abundance exceeding approximately 30%, or  $\sim 5\%$  surface area contribution, could potentially bias quantitative records.

An additional paleoceanographic implication to consider is the strong seasonal signal apparent in the data generated from a coastal Antarctic environment. The larger  $\delta^{15}\text{N}_{\text{DB-offset}}$  observed in summer samples, and thus larger potential impact of CRS on  $\delta^{15}\text{N}_{\text{DB}}$  records, may not be as apparent in open ocean sedimentary records, as summer productivity tends to be reduced relative to spring and therefore contributes less to the integrated sedimentary signal (Robinson et al., 2020). On the other hand, if the internal fractionation is related to light period and/or intensity, then increased exposure during interglacial periods could amplify potential CRS bias, albeit at time periods when CRS tend to be less abundant in Antarctic Zone sediments. Consideration of location-specific processes and further culture-based research into internal N isotope fractionation during resting spore formation is therefore necessary to better constrain CRS impact on  $\delta^{15}\text{N}_{\text{DB}}$  records.

## 5. Conclusions

Results from culture experiments and sedimentary measurements show that CRS record low  $\delta^{15}\text{N}_{\text{DB}}$  values relative to vegetative *Chaetoceros* and other diatoms. This is surprising because CRS form when nutrients are depleted and consequently when  $\delta^{15}\text{N}_{\text{NO}_3}$  is elevated. Low  $\delta^{15}\text{N}_{\text{DB}}$  values in CRS are tentatively attributed to ammonium assimilation, heavy silicification, and strong internal allocation processes, but additional research into CRS formation and silicification is necessary to provide further insights into such processes.

Nitrogen isotopic data from culture experiments and sediments, paired with diatom assemblage data, suggest that increased CRS abundance in open ocean sediments does not significantly bias two examples of  $\delta^{15}\text{N}_{\text{DB}}$  records spanning glacial-interglacial cycles. However, lower  $\delta^{15}\text{N}_{\text{DB}}$  values in CRS may be relevant to quantitative analyses of records with changes in CRS relative abundance exceeding approximately 30% (5% surface area contribution) and to  $\delta^{15}\text{N}_{\text{DB}}$  records generated in coastal regions, such as the Antarctic Peninsula, where CRS are especially abundant. Estimates of  $\delta^{15}\text{N}_{\text{DB}}$  biases over time due to changing diatom assemblages can be further honed with tighter constraint on CRS surface area or total N contribution and with similar studies of relevant species, such as *E. antarctica*. Ultimately, our work highlights the importance of considering diatom assemblage changes throughout sedimentary  $\delta^{15}\text{N}_{\text{DB}}$  records, especially when such records are applied for quantitative paleo reconstructions.

### Data Availability Statement

Data generated for this study are archived at the U.S. Antarctic Program Data Center. Data sets include measurements from culture experiments (Dove, 2023a), geochemical measurements from ODP Site 1098 (Dove, 2022), and diatom assemblages from ODP Site 1098 (Dove, 2023b).

### Acknowledgments

This work was supported by NSF OPP award 1744871 to R.S.R. N.R. received funding from NSF OCE award 1847509. Thanks to E. Baker and D. Outram of the Marine Science Research Facility for assistance with facilities and instrumentation necessary to maintain laboratory cultures. Thanks to S. Setta for assistance with isolating diatoms and to C. Gelfman, S. Lerch, and T. Rynearson for taking samples during experiment 2. Thank you to the curatorial staff at the Gulf Coast Repository for providing samples from ODP Site 1098. Finally, we thank two anonymous reviewers whose insightful feedback greatly improved this manuscript.

### References

- Abelmann, A., Gersonde, R., Cortese, G., Kuhn, G., & Smetacek, V. (2006). Extensive phytoplankton blooms in the Atlantic sector of the glacial Southern Ocean. *Paleoceanography*, 21(1), 1013. <https://doi.org/10.1029/2005PA001199>
- Ai, X. E., Studer, A. S., Sigman, D. M., Martínez-García, A., Fripiat, F., Thöle, L. M., et al. (2020). Southern Ocean upwelling, Earth's obliquity, and glacial-interglacial atmospheric CO<sub>2</sub> change. *Science*, 370(6522), 1348–1352. <https://doi.org/10.1126/science.abd2115>
- Allen, A. E., Dupont, C. L., Obornik, M., Horák, A., Nunes-Nesi, A., McCrow, J. P., et al. (2011). Evolution and metabolic significance of the urea cycle in photosynthetic diatoms. *Nature*, 473(7346), 203–207. <https://doi.org/10.1038/nature10074>
- Altabet, M. A., & Francois, R. (1994). Sedimentary nitrogen isotopic ratio as a recorder for surface ocean nitrate utilization. *Global Biogeochemical Cycles*, 8(1), 103–116. <https://doi.org/10.1029/93GB03396>
- Armand, L. K., Crosta, X., Romero, O., & Pichon, J. J. (2005). The biogeography of major diatom taxa in Southern Ocean sediments: 1. Sea ice related species. *Palaeoecology, Palaeoclimatology, Palaeoecology*, 223(1–2), 93–126. <https://doi.org/10.1016/J.PALAEO.2005.02.015>
- Bishop, I. W., Anderson, S. I., Collins, S., & Rynearson, T. A. (2022). Thermal trait variation may buffer Southern Ocean phytoplankton from anthropogenic warming. *Global Change Biology*, 28(19), 5755–5767. <https://doi.org/10.1111/GCB.16329>
- Bohrmann, G. (2019). The expedition PS119 of the research vessel POLARSTERN to Eastern Scotia Sea in 2019.
- Braman, R. S., & Hendrix, S. A. (1989). Nanogram nitrite and nitrate determination in environmental and biological materials by vanadium(III) reduction with chemiluminescence detection. *Analytical Chemistry*, 61(24), 2715–2718. <https://doi.org/10.1021/ac00199a007>
- Bromke, M. A. (2013). Amino acid biosynthesis pathways in diatoms. *Metabolites*, 3(2), 294–311. <https://doi.org/10.3390/METABO3020294>
- Brzezinski, M. A. (1985). The Si:C:N ratio of marine diatoms: Interspecific variability and the effect of some environmental variables. *Journal of Phycology*, 21(3), 347–357. <https://doi.org/10.1111/J.0022-3646.1985.00347.X>
- Civel-Mazens, M., Crosta, X., Cortese, G., Michel, E., Mazaud, A., Ther, O., et al. (2021). Impact of the agulhas return current on the oceanography of the Kerguelen Plateau region, Southern Ocean, over the last 40 kyrs. *Quaternary Science Reviews*, 251, 106711. <https://doi.org/10.1016/j.quascirev.2020.106711>
- Crosta, X., & Koç, N. (2007). Chapter eight diatoms: From micropaleontology to isotope geochemistry. *Developments in Marine Geology*, 1, 327–369. [https://doi.org/10.1016/S1572-5480\(07\)01013-5](https://doi.org/10.1016/S1572-5480(07)01013-5)
- Crosta, X., Pichon, J.-J., & Labracherie, M. (1997). Distribution of Chaetoceros resting spores in modern peri-Antarctic sediments. *Marine Micropaleontology*, 29(3–4), 283–299. [https://doi.org/10.1016/S0377-8398\(96\)00033-3](https://doi.org/10.1016/S0377-8398(96)00033-3)
- Denis, D., Crosta, X., Zaragosi, S., Romero, O., Martin, B., & Mas, V. (2006). Seasonal and subseasonal climate changes recorded in laminated diatom ooze sediments, Adélie Land, East Antarctica. *The Holocene*, 16(8), 1137–1147. <https://doi.org/10.1177/0959683606069414>
- Dove, I. (2022). Sediment chemistry of ODP Site 1098 [Dataset]. *U.S. Antarctic Program (USAP) Data Center*. <https://doi.org/10.15784/601778>
- Dove, I. (2023a). Dissolved nutrients, cell counts, and nitrogen isotope measurements from *Chaetoceros socialis* culture experiments [Dataset]. *U.S. Antarctic Program (USAP) Data Center*. <https://doi.org/10.15784/601727>
- Dove, I. (2023b). ODP Site 1098 deglacial diatom assemblage [Dataset]. *U.S. Antarctic Program (USAP) Data Center*. <https://doi.org/10.15784/601777>
- Egan, K. E., Rickaby, R. E. M., Leng, M. J., Hendry, K. R., Hermoso, M., Sloane, H. J., et al. (2012). Diatom silicon isotopes as a proxy for silicic acid utilisation: A Southern Ocean core top calibration. *Geochimica et Cosmochimica Acta*, 96, 174–192. <https://doi.org/10.1016/J.GCA.2012.08.002>
- Eppley, R. W., & Renger, E. H. (1974). Nitrogen assimilation of an oceanic diatom in nitrogen-limited continuous culture. *Journal of Phycology*, 10(1), 15–23. <https://doi.org/10.1111/J.1529-8817.1974.TB02671.X>
- Esper, O., Gersonde, R., & Kadagies, N. (2010). Diatom distribution in southeastern Pacific surface sediments and their relationship to modern environmental variables. *Palaeoecology, Palaeoclimatology, Palaeoecology*, 287(1–4), 1–27. <https://doi.org/10.1016/J.PALAEO.2009.12.006>
- French, F. W., & Hargraves, P. E. (1985). Spore formation in the life cycles of the diatoms *Chaetoceros diadema* and *Leptocylindrus danicus*. *Journal of Phycology*, 21(3), 477–483. <https://doi.org/10.1111/J.0022-3646.1985.00477.X>
- Fripiat, F., Sigman, D. M., Fawcett, S. E., Rafter, P. A., Weigand, M. A., & Tison, J. L. (2014). New insights into sea ice nitrogen biogeochemical dynamics from the nitrogen isotopes. *Global Biogeochemical Cycles*, 28(2), 115–130. <https://doi.org/10.1002/2013GB004729>
- Gersonde, R., Crosta, X., Abelmann, A., & Armand, L. (2005). Sea-Surface temperature and sea ice distribution of the Southern Ocean at the EPILOG last glacial maximum—A circum-Antarctic view based on siliceous microfossil records. *Quaternary Science Reviews*, 24(7–9), 869–896. <https://doi.org/10.1016/J.QUASCIREV.2004.07.015>

- Guillard, R. R. L. (1975). Culture of phytoplankton for feeding marine invertebrates. In W. L. Smith & M. H. Chanley (Eds.), *Culture of marine invertebrate animals* (pp. 29–60). Springer.
- Hasle, G. R., & Syvertsen, E. E. (1997). C. R. Tomas (Ed.), *Identifying marine phytoplankton*. Academic Press.
- Henley, S. F., Tuerena, R. E., Annett, A. L., Fallick, A. E., Meredith, M. P., Venables, H. J., et al. (2017). Macronutrient supply, uptake and recycling in the coastal ocean of the west Antarctic Peninsula. *Deep-Sea Research Part II Topical Studies in Oceanography*, *139*, 58–76. <https://doi.org/10.1016/j.dsr2.2016.10.003>
- Hildebrand, M., Lerch, S. J. L., & Shrestha, R. P. (2018). Understanding diatom cell wall silicification—moving forward. *Frontiers in Marine Science*, *5*(APR), 125. <https://doi.org/10.3389/FMARS.2018.00125/BIBTEX>
- Holmes, R. M., Aminot, A., K rouel, R., Hooker, B. A., & Peterson, B. J. (1999). A simple and precise method for measuring ammonium in marine and freshwater ecosystems. *Canadian Journal of Fish and Aquatic Sciences*, *56*(10), 1801–1808. <https://doi.org/10.1139/F99-128>
- Horn, M. G., Beucher, C. P., Robinson, R. S., & Brzezinski, M. A. (2011a). Southern ocean nitrogen and silicon dynamics during the last deglaciation. *Earth and Planetary Science Letters*, *310*(3–4), 334–339. <https://doi.org/10.1016/j.epsl.2011.08.016>
- Horn, M. G., Robinson, R. S., Rynearson, T. A., & Sigman, D. M. (2011b). Nitrogen isotopic relationship between diatom-bound and bulk organic matter of cultured polar diatoms. *Paleoceanography*, *26*(3), PA3208. <https://doi.org/10.1029/2010PA002080>
- Jacot Des Combes, H., Esper, O., De La Rocha, C. L., Abelmann, A., Gersonde, R., Yam, R., & Shemesh, A. (2008). Diatom  $\delta^{13}\text{C}$ ,  $\delta^{15}\text{N}$ , and C/N since the last glacial maximum in the Southern Ocean: Potential impact of species composition. *Paleoceanography*, *23*(4), PA4209. <https://doi.org/10.1029/2008PA001589>
- Jones, C. A., Closset, I., Riesselman, C. R., Kelly, R. P., Brzezinski, M. A., & Robinson, R. S. (2022). New constraints on assemblage-driven variation in the relationship amongst diatom-bound, biomass, and nitrate nitrogen isotope values. *Paleoceanography and Paleoclimatology*, *37*(8), e2022PA004428. <https://doi.org/10.1029/2022pa004428>
- Kemeny, P. C., Kast, E. R., Hain, M. P., Fawcett, S. E., Fripiat, F., Studer, A. S., et al. (2018). A seasonal model of nitrogen isotopes in the ice age Antarctic Zone: Support for weakening of the Southern Ocean upper overturning cell. *Paleoceanography and Paleoclimatology*, *33*(12), 1453–1471. <https://doi.org/10.1029/2018PA003478>
- Knapp, A. N., Sigman, D. M., & Lipschultz, F. (2005). N isotopic composition of dissolved organic nitrogen and nitrate at the Bermuda Atlantic Time-series study site. *Global Biogeochemical Cycles*, *19*(1), 1–15. <https://doi.org/10.1029/2004GB002320>
- Knox, F., & McElroy, M. B. (1984). Changes in atmospheric  $\text{CO}_2$  influence of the marine biota at high latitude. *Journal of Geophysical Research*, *89*(D3), 4629–4637. <https://doi.org/10.1029/jd089id03p04629>
- Kotzsch, A., Gr ger, P., Pawolowski, D., Bomans, P. H. H., Sommerdijk, N. A. J. M., Schlierf, M., & Kr ger, N. (2017). Silicanin-1 is a conserved diatom membrane protein involved in silica biomineralization. *BMC Biology*, *15*(1), 65. <https://doi.org/10.1186/S12915-017-0400-8>
- Kr ger, N., Deutzmann, R., Bergsdorf, C., & Sumper, M. (2000). Species-specific polyamines from diatoms control silica morphology. *Proceedings of the National Academy of Sciences of the United States of America*, *97*(26), 14133–14138. <https://doi.org/10.1073/PNAS.260496497>
- Kr ger, N., Deutzmann, R., & Sumper, M. (1999). Polycationic peptides from diatom biosilica that direct silica nanosphere formation. *Science*, *286*(5442), 1129–1132. <https://doi.org/10.1126/SCIENCE.286.5442.1129>
- Kr ger, N., & Poulsen, N. (2008). Diatoms - from cell wall biogenesis to nanotechnology. *Annual Review of Genetics*, *42*, 83–107. <https://doi.org/10.1146/ANNUREV.GENET.41.110306.130109/CITE/REFWORKS>
- Kuwata, A., Hama, T., & Takahashi, M. (1993). Ecophysiological characterization of two life forms, resting spores and resting cells, of a marine planktonic diatom, *Chaetoceros pseudocurvisetus*, formed under nutrient depletion. *Marine Ecology Progress Series*, *102*, 245–255. <https://doi.org/10.3354/meps102245>
- Leblanc, K., Aristegui, J., Armand, L., Assmy, P., Beker, B., Bode, A., et al. (2012). A global diatom database - Abundance, biovolume and biomass in the world ocean. *Earth System Science Data Discussions*, *5*, 147–185. <https://doi.org/10.5194/essdd-5-147-2012>
- Leventer, A. (1991). Sediment trap diatom assemblages from the northern Antarctic Peninsula region. *Deep-Sea Research, Part A: Oceanographic Research Papers*, *38*(8–9), 1127–1143. [https://doi.org/10.1016/0198-0149\(91\)90099-2](https://doi.org/10.1016/0198-0149(91)90099-2)
- Maddison, E. J., Pike, J., Leventer, A., & Domack, E. W. (2005). Deglacial seasonal and sub-seasonal diatom record from Palmer Deep, Antarctica. *Journal of Quaternary Science*, *20*(5), 435–446. <https://doi.org/10.1002/JQS.947>
- Martin, J. H. (1990). Glacial-interglacial  $\text{CO}_2$  change: The iron hypothesis. *Paleoceanography*, *5*(1), 1–13. <https://doi.org/10.1029/PA0051001P00001>
- Mart nez-Garc a, A., Sigman, D. M., Ren, H., Anderson, R. F., Straub, M., Hodell, D. A., et al. (2014). Iron fertilization of the subantarctic ocean during the last ice age. *Science*, *343*(6177), 1347–1350. [https://doi.org/10.1126/SCIENCE.1246848/SUPPL\\_FILE/MARTINEZ-GARCIA.SM.PDF](https://doi.org/10.1126/SCIENCE.1246848/SUPPL_FILE/MARTINEZ-GARCIA.SM.PDF)
- McNair, H. M., Brzezinski, M. A., Till, C. P., & Krause, J. W. (2018). Taxon-specific contributions to silica production in natural diatom assemblages. *Limnology & Oceanography*, *63*(3), 1056–1075. <https://doi.org/10.1002/LNO.10754>
- Mitchell, B. G., Brody, E. A., Holm-Hansen, O., McClain, C., & Bishop, J. (1991). Light limitation of phytoplankton biomass and macronutrient utilization in the Southern Ocean. *Limnology & Oceanography*, *36*(8), 1662–1677. <https://doi.org/10.4319/LO.1991.36.8.1662>
- Morales, L. v., Granger, J., Chang, B. X., Prokopenko, M. G., Plessen, B., Gradinger, R., & Sigman, D. M. (2014). Elevated  $^{15}\text{N}/^{14}\text{N}$  in particulate organic matter, zooplankton, and diatom frustule-bound nitrogen in the ice-covered water column of the Bering Sea eastern shelf. *Deep Sea Research Part II: Topical Studies in Oceanography*, *109*, 100–111. <https://doi.org/10.1016/j.dsr2.2014.05.008>
- Morales, L. V., Sigman, D. M., Horn, M. G., & Robinson, R. S. (2013). Cleaning methods for the isotopic determination of diatom-bound nitrogen in non-fossil diatom frustules. *Limnology and Oceanography: Methods*, *11*(2), 101–112. <https://doi.org/10.4319/lom.2013.11.101>
- Nielsen, S. (2004). *Southern Ocean climate variability*. University of Troms  and Norwegian Polar Institute.
- Oku, O., & Kamatani, A. (1997). Resting spore formation of the marine planktonic diatom *Chaetoceros anastomosans* induced by high salinity and nitrogen depletion. *Marine Biology*, *127*(3), 515–520. <https://doi.org/10.1007/s002270050040>
- Orsi, A., Whitworth, T., III, & Nowlin, W., Jr. (1995). On the meridional extent and fronts of the Antarctic Circumpolar Current. *Deep Sea Research Part I: Oceanographic Research Papers*, *42*(5), 641–673. [https://doi.org/10.1016/0967-0637\(95\)00021-w](https://doi.org/10.1016/0967-0637(95)00021-w)
- Pelusi, A., Santelia, M. E., Benevenuto, G., Godhe, A., & Montresor, M. (2020). The diatom *Chaetoceros socialis*: Spore formation and preservation. *European Journal of Phycology*, *55*(1), 1–10. <https://doi.org/10.1080/09670262.2019.1632935>
- Penna, A., Magnani, M., Fenoglio, I., Fubini, B., Cerrano, C., Giovine, M., & Bavestrello, G. (2003). Marine diatom growth on different forms of particulate silica: Evidence of cell/particle interaction. *Aquatic Microbial Ecology*, *32*(3), 299–306. <https://doi.org/10.3354/AME032299>
- Pichon, J. J., Bareille, G., Labracherie, M., Labeyrie, L. D., Baudrimont, A., & Turon, J. L. (1992). Quantification of the biogenic silica dissolution in Southern Ocean Sediments. *Quaternary Research*, *37*(3), 361–378. [https://doi.org/10.1016/0033-5894\(92\)90073-R](https://doi.org/10.1016/0033-5894(92)90073-R)
- Reagan, J., Boyer, T., Garc a, H., Locarnini, R., Baranova, O., Bouchard, C., et al. (2024). World Ocean Atlas 23.

- Rembauville, M., Manno, C., Tarling, G. A., Blain, S., & Salter, I. (2016). Strong contribution of diatom resting spores to deep-sea carbon transfer in naturally iron-fertilized waters downstream of South Georgia. *Deep-Sea Research Part I Oceanographic Research Papers*, *115*, 22–35. <https://doi.org/10.1016/j.dsr.2016.05.002>
- Rigual-Hernández, A. S., Trull, T. W., Bray, S. G., Cortina, A., & Armand, L. K. (2015). Latitudinal and temporal distributions of diatom populations in the pelagic waters of the Subantarctic and Polar Frontal zones of the Southern Ocean and their role in the biological pump. *Biogeosciences*, *12*(18), 5309–5337. <https://doi.org/10.5194/BG-12-5309-2015>
- Robinson, R. S., Brunelle, B. G., & Sigman, D. M. (2004). Revisiting nutrient utilization in the glacial Antarctic: Evidence from a new method for diatom-bound N isotopic analysis. *Paleoceanography*, *19*(3), PA3001. <https://doi.org/10.1029/2003PA000996>
- Robinson, R. S., Jones, C. A., Dove, I. A., Kelly, R. P., & Brzezinski, M. A. (2025). Monospecific diatom cultures suggest potential interspecies variation of diatom-bound nitrogen isotope signatures associated with silica acquisition. *Geochemistry, Geophysics, Geosystems*, *26*(2), e2024GC011923. <https://doi.org/10.1029/2024GC011923>
- Robinson, R. S., Jones, C. A., Kelly, R. P., Love, A., Closset, I., Rafter, P. A., & Brzezinski, M. (2020). A test of the diatom-bound paleoproxy: Tracing the isotopic composition of nutrient-nitrogen into Southern Ocean particles and sediments. *Global Biogeochemical Cycles*, *34*(10), e2019GB006508. <https://doi.org/10.1029/2019GB006508>
- Robinson, R. S., & Sigman, D. M. (2008). Nitrogen isotopic evidence for a poleward decrease in surface nitrate within the ice age Antarctic. *Quaternary Science Reviews*, *27*(9–10), 1076–1090. <https://doi.org/10.1016/j.quascirev.2008.02.005>
- Robinson, R. S., Sigman, D. M., DiFiore, P. J., Rohde, M. M., Mashiotta, T. A., & Lea, D. W. (2005). Diatom-bound 15N/14N: New support for enhanced nutrient consumption in the ice age subantarctic. *Paleoceanography*, *20*(3), 1–14. <https://doi.org/10.1029/2004PA001114>
- Ryneason, T. A., Richardson, K., Lampitt, R. S., Sieracki, M. E., Poulton, A. J., Lyngsgaard, M. M., & Perry, M. J. (2013). Major contribution of diatom resting spores to vertical flux in the sub-polar North Atlantic. *Deep Sea Research Part I: Oceanographic Research Papers*, *82*, 60–71. <https://doi.org/10.1016/j.dsr.2013.07.013>
- Saito, H., & Tsuda, A. (2003). Influence of light intensity on diatom physiology and nutrient dynamics in the Oyashio region. *Progress in Oceanography*, *57*(3–4), 251–263. [https://doi.org/10.1016/S0079-6611\(03\)00100-9](https://doi.org/10.1016/S0079-6611(03)00100-9)
- Sarmiento, J. L., & Toggweiler, J. R. (1984). A new model for the role of the oceans in determining atmospheric pCO<sub>2</sub>. *Nature*, *308*(5960), 621–624. <https://doi.org/10.1038/308621a0>
- Scherer, R. (1994). A new method for the determination of absolute abundance of diatoms and other silt-sized sedimentary particles. *Journal of Paleolimnology*, *12*(2), 171–179. <https://doi.org/10.1007/bf00678093>
- Schweitzer, P. N. (1995). Monthly averaged polar sea-ice concentration. *Nature*, *308*(5960), 624–626. <https://doi.org/10.1038/308624a0>
- Siegenthaler, U., & Wenk, T. (1984). Rapid atmospheric CO<sub>2</sub> variations and ocean circulation. *Nature*, *308*(5960), 624–626. <https://doi.org/10.1038/308624a0>
- Sigman, D. M., Altabet, M. A., Francois, R., McCorkle, D. C., & Gaillardet, J. F. (1999). The isotopic composition of diatom-bound nitrogen in Southern Ocean sediments. *Paleoceanography*, *14*(2), 118–134. <https://doi.org/10.1029/1998PA000018>
- Sigman, D. M., Casciotti, K. L., Andreani, M., Barford, C., Galanter, M., & Böhlke, J. K. (2001). A bacterial method for the nitrogen isotopic analysis of nitrate in seawater and freshwater. *Analytical Chemistry*, *73*(17), 4145–4153. <https://doi.org/10.1021/AC010088E/ASSET/IMAGES/LARGE/AC010088EF00006.JPEG>
- Sigman, D. M., Hain, M. P., & Haug, G. H. (2010). The polar ocean and glacial cycles in atmospheric CO<sub>2</sub> concentration. *Nature*, *466*(7302), 47–55. <https://doi.org/10.1038/nature09149>
- Smetacek, V., Klaas, C., Strass, V. H., Assmy, P., Montresor, M., Cisewski, B., et al. (2012). Deep carbon export from a Southern Ocean iron-fertilized diatom bloom. *Nature*, *487*(7407), 313–319. <https://doi.org/10.1038/nature11229>
- Strickland, J., & Parsons, T. (1972). *A practical handbook of seawater analysis* (2nd ed.). Fisheries Research Board of Canada.
- Studer, A. S., Ellis, K. K., Oleynik, S., Sigman, D. M., & Haug, G. H. (2013). Size-specific opal-bound nitrogen isotope measurements in North Pacific sediments. *Geochimica et Cosmochimica Acta*, *120*, 179–194. <https://doi.org/10.1016/j.gca.2013.06.041>
- Studer, A. S., Sigman, D. M., Martínez-García, A., Benz, V., Winckler, G., Kuhn, G., et al. (2015). Antarctic Zone nutrient conditions during the last two glacial cycles. *Paleoceanography*, *30*(7), 845–862. <https://doi.org/10.1002/2014PA002745>
- Sumper, M., & Kröger, N. (2004). Silica formation in diatoms: The function of long-chain polyamines and silaffins. *Journal of Materials Chemistry*, *14*(14), 2059–2065. <https://doi.org/10.1039/B401028K>
- Swann, G. E. A., Pike, J., Snelling, A. M., Leng, M. J., & Williams, M. C. (2013). Seasonally resolved diatom δ18O records from the West Antarctic Peninsula over the last deglaciation. *Earth and Planetary Science Letters*, *364*, 12–23. <https://doi.org/10.1016/j.epsl.2012.12.016>
- Taylor, F., & Sjunneskog, C. (2002). Postglacial marine diatom record of the Palmer Deep, Antarctic Peninsula (ODP Leg 178, Site 1098) 2. Diatom assemblages. *Paleoceanography*, *17*(3). <https://doi.org/10.1029/2000PA000564>
- Tesson, B., Lerch, S. J. L., & Hildebrand, M. (2017). Characterization of a new protein family associated with the silica deposition vesicle membrane enables genetic manipulation of diatom silica. *Scientific Reports* *2017*, *7*(1), 1–13. <https://doi.org/10.1038/s41598-017-13613-8>
- Tréguer, P., Bowler, C., Moriceau, B., Dutkiewicz, S., Gehlen, M., Aumont, O., et al. (2018). Influence of diatom diversity on the ocean biological carbon pump. *Nature Geoscience*, *11*(1), 27–37. <https://doi.org/10.1038/s41561-017-0028-x>
- Wada, E., & Hattori, A. (1978). Nitrogen isotope effects in the assimilation of inorganic nitrogenous compounds by marine diatoms. *Geomicrobiology Journal*, *1*(1), 85–101. <https://doi.org/10.1080/01490457809377725>
- Werner, R. A., & Schmidt, H. L. (2002). The in vivo nitrogen isotope discrimination among organic plant compounds. *Phytochemistry*, *61*(5), 465–484. [https://doi.org/10.1016/S0031-9422\(02\)00204-2](https://doi.org/10.1016/S0031-9422(02)00204-2)
- Yodsuwan, N., Sawayama, S., & Sirisansaneeyakul, S. (2017). Effect of nitrogen concentration on growth, lipid production and fatty acid profiles of the marine diatom *Phaeodactylum tricornutum*. *Agriculture and Natural Resources*, *51*(3), 190–197. <https://doi.org/10.1016/J.ANRES.2017.02.004>
- Zielinski, U., & Gersonde, R. (1997). Diatom distribution in Southern Ocean surface sediments (Atlantic sector): Implications for paleoenvironmental reconstructions. *Palaeogeography, Palaeoclimatology, Palaeoecology*, *129*(3–4), 213–250. [https://doi.org/10.1016/S0031-0182\(96\)00130-7](https://doi.org/10.1016/S0031-0182(96)00130-7)
- Zimmermann, S. E., Benstein, R. M., Flores-Torero, M., Blau, S., Anoman, A. D., Rosa-Téllez, S., et al. (2021). The phosphorylated pathway of serine biosynthesis links plant growth with nitrogen metabolism. *Plant Physiology*, *186*(3), 1487–1506. <https://doi.org/10.1093/PLPHYS/KIAB167>